ARTICLE

https://doi.org/10.1038/s41586-019-1278-0

Atypical behaviour and connectivity in *SHANK3*-mutant macaques

Yang Zhou[1,2,12,13], Jitendra Sharma[3,4,5,6,13], Qiong Ke[7,8,13], Rogier Landman[2,9,13], Jingli Yuan[10], Hong Chen[7], David S. Hayden[11], John W. Fisher III[11], Minqing Jiang[1], William Menegas[2], Tomomi Aida[2], Ting Yan[1], Ying Zou[1], Dongdong Xu[1], Shivangi Parmar[2,3], Julia B. Hyman[2,3], Adrian Fanucci-Kiss[2,3], Olivia Meisner[2,3], Dongqing Wang[2,3], Yan Huang[10], Yaqing Li[10], Yanyang Bai[1], Wenjing Ji[1], Xinqiang Lai[7], Weiqiang Li[7,8], Lihua Huang[7], Zhonghua Lu[1], Liping Wang[1], Sheeba A. Anteraper[2,3], Mriganka Sur[3,4,5], Huihui Zhou[1]*, Andy Peng Xiang[7,8]*, Robert Desimone[2,3], Guoping Feng[2,3,9]* & Shihua Yang[10]*

Mutation or disruption of the SH3 and ankyrin repeat domains 3 (*SHANK3*) gene represents a highly penetrant, monogenic risk factor for autism spectrum disorder, and is a cause of Phelan–McDermid syndrome. Recent advances in gene editing have enabled the creation of genetically engineered non-human-primate models, which might better approximate the behavioural and neural phenotypes of autism spectrum disorder than do rodent models, and may lead to more effective treatments. Here we report CRISPR–Cas9-mediated generation of germline-transmissible mutations of *SHANK3* in cynomolgus macaques (*Macaca fascicularis*) and their F1 offspring. Genotyping of somatic cells as well as brain biopsies confirmed mutations in the *SHANK3* gene and reduced levels of SHANK3 protein in these macaques. Analysis of data from functional magnetic resonance imaging revealed altered local and global connectivity patterns that were indicative of circuit abnormalities. The founder mutants exhibited sleep disturbances, motor deficits and increased repetitive behaviours, as well as social and learning impairments. Together, these results parallel some aspects of the dysfunctions in the *SHANK3* gene and circuits, as well as the behavioural phenotypes, that characterize autism spectrum disorder and Phelan–McDermid syndrome.

SHANK3 encodes major scaffolding proteins at excitatory synapses, coordinates the recruitment of signalling molecules and creates scaffolds for appropriate alignment of glutamatergic neurotransmitter receptors, which promotes the development and maturation of excitatory synapses[1,2]. Mutation of *SHANK3* accounts for about 1% of idiopathic forms of autism spectrum disorder, and disruption of *SHANK3* is a major cause of neurodevelopmental deficits in Phelan–McDermid syndrome[3–6]. Patients with a *SHANK3* gene mutation often exhibit a variety of comorbid traits, which include global developmental delay, severe sleep disturbances, lack of speech or severe language delay, and characteristic features of autism spectrum disorder (such as social impairments and stereotypies)[7–9]. Previous studies in flies, fish and rodents have uncovered impaired synaptic function and several behavioural abnormalities due to loss of SHANK3[2,10,11]. For example, common abnormalities in *Shank3*-mutant mice include self-injury, repetitive grooming, reduced interaction with conspecifics, motor difficulties and increased levels of anxiety. However, it is increasingly apparent that the validity of *Shank3*-mutant rodent models for human patients is limited, in part owing to the fact that the aberrant behavioural phenotypes in mice are found almost exclusively in homozygous mutants and are barely detectable in heterozygous mutants[2,12]. In addition, social interactions between humans involve integrated cognition and comprehension, which are more closely associated in primates than in rodents[13–16]. There is therefore an urgent need to develop primate models of autism spectrum disorder to facilitate neurobiological studies and the development of therapies[12,13,17].

Cynomolgus monkeys (*M. fascicularis*) possess a high level of cognitive ability and complex social behaviour, and are closer to humans in terms of their brain structure and function than are rodents[12,13,16,17]. There has been great interest in using macaques as a non-human-primate model for studying brain disorders[17–20]. Recent advances in CRISPR–Cas9-mediated gene-editing technology have resulted in an increasingly efficient and reliable method for targeted gene disruption, which is highly suited to the creation of non-human-primate models of autism spectrum disorder[21,22]. Previous attempts to create a transgenic *SHANK3* macaque model have been hindered by the early death of the mutant founders[23], or by the fact that only a single mutant survived[24]—group comparisons are not possible with only a single mutant. A viable primate model of *SHANK3* mutation should include validation of the loss of protein isoforms, and functional and behavioural deficits should be present at the group level. Furthermore, germline transmission of CRISPR–Cas9-edited macaque genomes has yet to be fully demonstrated. Here we report the creation of a *SHANK3*-mutant macaque model with a specific target locus that—in human studies—has been linked to Phelan–McDermid syndrome and autism spectrum disorder. We also demonstrate the resultant functional and behavioural abnormalities using assays that can be adapted for testing with autism spectrum disorder and Phelan–McDermid syndrome in human patients. Furthermore, we successfully obtained an

[1]Brain Cognition and Brain Disease Institute, Shenzhen Institutes of Advanced Technology, Chinese Academy of Sciences, Shenzhen, China. [2]McGovern Institute for Brain Research, Massachusetts Institute of Technology, Cambridge, MA, USA. [3]Department of Brain and Cognitive Sciences, Massachusetts Institute of Technology, Cambridge, MA, USA. [4]Picower Institute for Learning and Memory, Massachusetts Institute of Technology, Cambridge, MA, USA. [5]Simons Center for the Social Brain, Massachusetts Institute of Technology, Cambridge, MA, USA. [6]Athinoula A. Martinos Center for Biomedical Imaging, Department of Radiology, Massachusetts General Hospital, Charlestown, MA, USA. [7]Center for Stem Cell Biology and Tissue Engineering, Key Laboratory for Stem Cells and Tissue Engineering, Sun Yat-Sen University, Guangzhou, China. [8]Guangzhou Regenerative Medicine and Health Guangdong Laboratory, Guangzhou, China. [9]Stanley Center for Psychiatric Research, Broad Institute of MIT and Harvard, Cambridge, MA, USA. [10]College of Veterinary Medicine, South China Agricultural University, Guangzhou, China. [11]Computer Science and Artificial Intelligence Laboratory, Massachusetts Institute of Technology, Cambridge, MA, USA. [12]Present address: Montreal Neurological Institute & Hospital, Department of Neurology and Neurosurgery, McGill University, Montreal, Quebec, Canada. [13]These authors contributed equally: Yang Zhou, Jitendra Sharma, Qiong Ke, Rogier Landman. *e-mail: hh.zhou@siat.ac.cn; xiangp@mail.sysu.edu.cn; fengg@mit.edu; yangsh@scau.edu.cn

F1 generation that has a homogenous pattern of *SHANK3* mutation, using sperm from CRISPR-edited founders.

Germline-transmissible *SHANK3* mutation in macaques

We applied a CRISPR–Cas9 strategy that targets exon 21 of the macaque *SHANK3* gene (Extended Data Fig. 2a). Exon 21 is the largest coding region of *SHANK3*, with numerous rare variants and point mutations in individuals with autism spectrum disorder[2–5,7]. We created indels in exon 21 analogous to the human autism spectrum disorder-linked InsG3680 mutation[25] that were previously generated and analysed in mice[26,27]. *Streptococcus pyogenes* Cas9 and two guide (g)RNAs were introduced to generate the mutation, and the successful creation of insertions or deletions (indels) were verified (Extended Data Fig. 2b, c). We transferred injected embryos into recipient females, and obtained five live newborns (labelled M1 to M5) that carried *SHANK3* mutations (Extended Data Fig. 2d). Four out of the five mutants (M1, M2, M3 and M5) are male, and one mutant (M4) is female. Genotyping of *SHANK3* from the newborns revealed several types of indel mutations in the *SHANK3* gene (Fig. 1a, Extended Data Fig. 3). M2 and M5 did not show a wild-type allele in genomic DNA; they are homozygous and compound-heterozygous, respectively (Fig. 1a, Extended Data Fig. 3). M1, M3 and M4 carried wild-type alleles in about 50% of the sequenced clones and thus are heterozygous, with (M1 and M3) or without (M4) genetic mosaicism (more than one type of indel). The control group consisted of age- and sex-matched macaques from the same colony. The general health measurements of the *SHANK3*-mutant macaques (such as body weight) were not different from controls (Extended Data Fig. 2e). Body condition scores of control and mutant groups were within the normal range for this species.

Sequencing results in exon 21 of the *SHANK3* gene showed multiple genotypes, which suggests that the CRISPR–Cas9-mediated cleavage of *SHANK3* resulted in a mosaicism of indels, as has previously been reported[21,22]. All of the indels from *SHANK3* mutants caused frameshift and loss-of-function mutations, except for a 12-bp in-frame deletion in mutant M4 and a 96-bp deletion in mutant M3; these led to a loss of 4 and 32 amino acids, respectively, within the proline-rich domain of SHANK3, which might be critical for the stability of SHANK3 protein isoforms and their interaction with scaffolds or receptors[1,2,7]. To determine how mutations of *SHANK3* affected the protein products of this gene, we biopsied tissue from primary visual cortex and performed western blot analysis. The biopsies were performed after completion of all behavioural tests and magnetic resonance imaging (MRI) scanning. We confirmed a decreased level of the isoforms of the SHANK3 protein in all five mutant monkeys (Fig. 1b, c, Extended Data Figs. 1 and 4) and thus validated the successful targeted disruption of exon 21, which has previously been linked to synaptic and circuit dysfunction[2,11,26,27].

To test for off-target modifications, we amplified and sequenced the top 20 genomic loci that were predicted by the Cas-OFFinder algorithm[28]. We analysed the sequencing results of these 20 loci from all 5 *SHANK3* mutants and confirmed their wild-type identities (Supplementary Table 1). Our data support the high fidelity of gene editing with CRISPR–Cas9, which aligns with previous surveys of CRISPR-edited model organisms[22].

To assess the germline transmission of the mutation, we collected and analysed the DNA of sperm from M2 (homozygous) and M3 (heterozygous and mosaic). We detected *SHANK3* mutations in the DNA of sperm cells of both individuals, and the patterns of mutation were similar to their respective somatic cells (Fig. 1d, Extended Data Figs. 1, 2f). We then performed intracytoplasmic sperm injection into wild-type oocytes using semen from monkey M2 (homozygous), and detected a 40-bp deletion mutation in all fertilized embryos (Fig. 1e, Extended Data Fig. 1). We successfully obtained live births of F1-generation mutant macaques after transferring the fertilized embryos. Genotyping of F1-generation mutant monkeys from the first cohort (labelled F1-1, F1-2 and F1-3) revealed a similar ratio of wild-type to mutant allele (labelled 'del 40 bp') from all three monkeys (Fig. 1f, Extended Data Fig. 1), which indicates that these are heterozygous *SHANK3*-mutant monkeys without genetic mosaicism. Taken together, these results show that the simultaneous delivery of two gRNAs that target both strands of exon 21 enables the efficient mutagenesis of *SHANK3* and the germline transmission of the mutant allele, in cynomolgus monkeys.

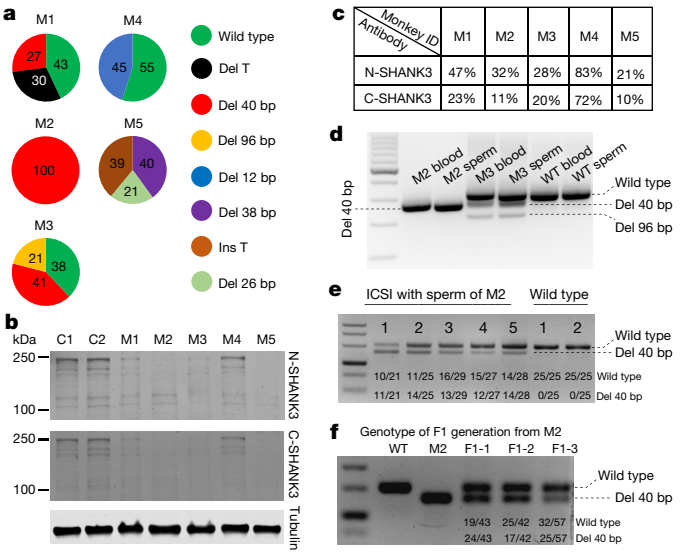

Monkey ID / Antibody	M1	M2	M3	M4	M5
N-SHANK3	47%	32%	28%	83%	21%
C-SHANK3	23%	11%	20%	72%	10%

Fig. 1 | Generation and germline transmission of macaques with *SHANK3* mutations. a, Pie charts of genotype (indels) from cultured skin fibroblasts derived from each mutant monkey. **b**, Representative western blots using brain lysates prepared from a V1 biopsy of two wild-type macaques (labelled C1 (male) and C2 (female)) and all five mutants (M1–M5), probed with N-terminal and C-terminal antibodies, and α-tubulin as loading control on the same gel. **c**, Relative levels of SHANK3 proteins calculated by averaging five technical repeats with the same V1 biopsy sample, and normalizing to α-tubulin loading controls. **d**, Genotyping PCR results of *SHANK3* from DNA from blood and sperm samples collected from M2, M3 and a wild-type (WT) control. **e**, Top, genotyping PCR results of *SHANK3* from individual cultured embryos after intracytoplasmic injection of single sperm (ICSI) from M2 and a wild-type control. Bottom, numbers of reads for wild-type and a 40-bp deletion are presented by Sanger sequencing of each bacterial colony after cloning of PCR products into sequencing vector. **f**, Top, genotyping PCR results of three live-birth, F1-generation monkeys after ICSI of sperm from M2. Bottom, numbers of reads for wild-type and a 40-bp deletion for each monkey (F1-1, F1-2 and F2-3) by Sanger sequencing of cloned PCR products.

Altered sleep, home cage activity and muscle tone

Patients with Phelan–McDermid syndrome and other individuals with *SHANK3* mutations often exhibit a variety of traits, which include motor impairment, severe sleep disturbances, lack of speech or severe language delay, abnormal sensory processing, intellectual disability, muscular hypotonia and seizure, as well as other symptomologies[2–8]. Most patients with Phelan–McDermid syndrome also exhibit stereotypies, and impairments in social interaction[4,8]. We used a panel of behavioural tests to examine phenotypes associated with *SHANK3* mutation in macaques. All observations, scoring and data analysis for these tests were carried out by researchers who were blinded to experimental design, goals and genotypes.

To assess sleep disturbance in the mutant monkeys, we habituated them to wearing an actigraphy device. The activity data revealed that overall activity levels were substantially reduced in mutant monkeys compared to controls (Fig. 2a–g). Mutant monkeys displayed a longer latency to sleep than controls, and an increased frequency of waking (as indicated by a fragmentation index) (Fig. 2h, i). These results showed a reduction in overall sleep efficiency in *SHANK3*-mutant monkeys (Fig. 2j, Extended Data Fig. 5).

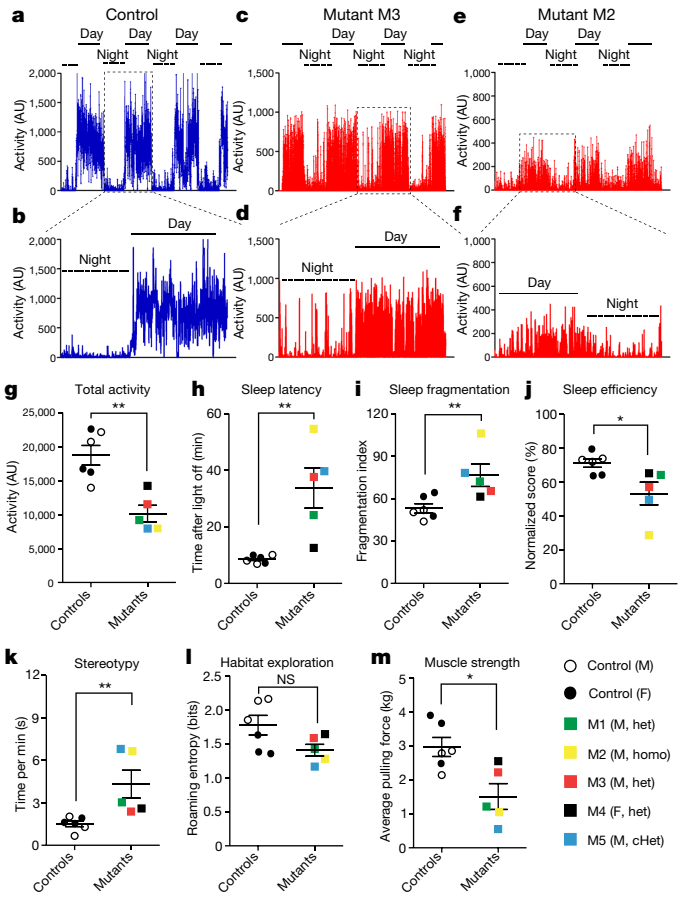

Fig. 2 | Sleep disturbances and altered home-cage activity in *SHANK3*-mutant macaques. a, **c**, **e**, Representative traces of overall activity recorded by a motion watch across multiple days from a control macaque and two mutants. AU, arbitrary units. **b**, **d**, **f**, Enlarged traces of overall activity recorded by motion watch over the course of 24 h from a control macaque, M3 and M2. **g**, Reduced overall activity in *SHANK3* mutants. **h**, Increased latency to fall asleep in *SHANK3* mutants. **i**, Increased fragmentation of sleep in *SHANK3* mutants during the night. **j**, Reduced efficiency of sleep in *SHANK3* mutants during the night. **k**, Increased time spent on stereotypic behaviours, presented as seconds per minute, in *SHANK3* mutants. **l**, *SHANK3* mutants show a trend of reduced area exploration in their home cages, as defined by roaming entropy. **m**, *SHANK3* mutants display reduced muscle strength. In **g**–**m**, $n = 6$ macaques for control group; $n = 5$ macaques for the *SHANK3*-mutant group; P value $= 0.0087$ (**g**), 0.0043 for (**h**), 0.0087 (**i**), 0.0303 (**j**), 0.0043 (**k**), 0.08 (**l**) and 0.03 (**m**). Data are presented as mean ± s.e.m. Two-tailed Mann–Whitney U-test. Coloured squares indicate individual monkeys with *SHANK3* mutation. M, male; F, female, het, heterozygous; homo, homozygous; cHet, compound heterozygous.

We recorded daily home-cage videos and scored behavioural variables using Noldus Observer software (see representative ethograms in Supplementary Table 2). The mutant macaques showed a substantial increase in stereotyped or repetitive behaviours compared to controls, as indicated by increased back-flipping, finger licking and biting of cage bars (Fig. 2k). In contrast to the increased amount of self-injurious grooming that is consistently observed in *Shank3*-mutant mice, the stereotypy in *SHANK3*-mutant monkeys was diverse. For instance, repetitive flipping was observed in mutant M3, whereas M2 and M5 displayed a pronounced licking of fingers and cage bars. The mutant macaques also displayed a trend for reduced level of exploration of cage subdivisions, as demonstrated by roaming entropy (Fig. 2l).

To test for hypotonia, we habituated the monkeys to pull a digital scale and recorded their pulling force. The average pulling force was reduced in the mutant group (Fig. 2m).

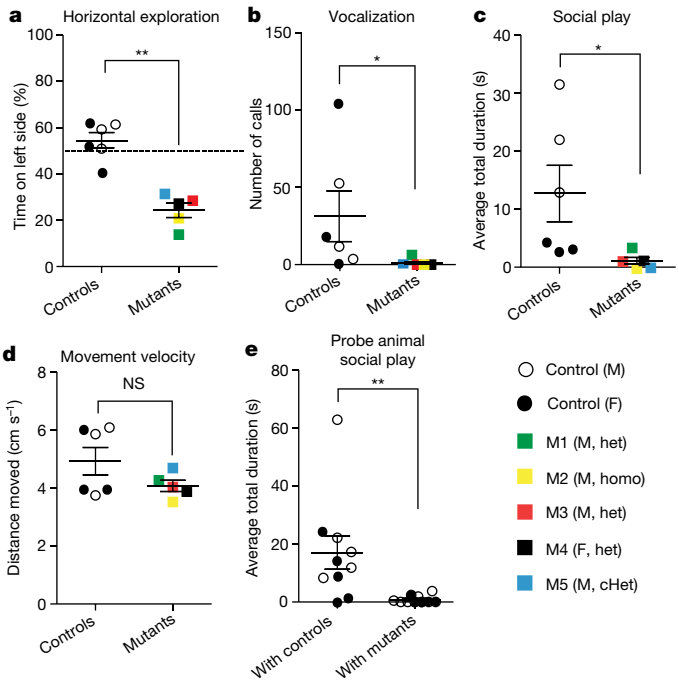

Fig. 3 | Impaired social interaction and reduced vocalization in *SHANK3* mutants. a, Proportion of time spent on the left versus right side of the cage shows that mutants tended to stay on one side, whereas control monkeys spent a roughly equal amount of time on each side. **b**, *SHANK3*-mutant monkeys made fewer vocalizations during the habituation period than did controls. **c**, Average total duration of aggregate social behaviours (which included chasing, following, fleeing, circling and play) was lower in mutants than in controls. **d**, No difference in movement velocity during the social test between mutants and controls. **e**, Average total duration of aggregate social behaviours was reduced in probe monkeys (wild type) when paired with *SHANK3* mutants, compared to probe monkeys paired with controls. $n = 6$ macaques for wild-type control group; $n = 5$ macaques for *SHANK3*-mutant group; in **e**, $n = 10$ wild-type macaques (five males, five females and age-matched to experimental animals) for probe monkeys. $P = 0.0043$ (**a**), 0.0444 (**b**), 0.0173 (**c**) and 0.0023 (**e**). NS, not significant. Data are presented as mean ± s.e.m. Two-tailed Mann–Whitney U-test. Coloured squares indicate individual monkeys with *SHANK3* mutation.

Impaired social interaction

We designed a paired social interaction assay between juvenile monkeys. The monkeys were habituated in the test cage before the social test began (Extended Data Fig. 6a). During habituation, the mutant macaques showed a reduced amount of exploration in the horizontal plane (Fig. 3a). Vocalization during the 20 minutes of habituation was reduced in the mutants (Fig. 3b). In the social interaction test, the scoring of detailed activities for the first five minutes revealed that mutants spent less time on aggregate social behaviours, which included chasing, following, circling, fleeing and play (Fig. 3c, Extended Data Fig. 6b–f). The mean velocity values during the social interactions were similar between the mutant and control monkeys (Fig. 3d), which suggests that physical limitations were unlikely to be major contributing factors to the reduced levels of social interaction. Furthermore, there was no difference in time spent on other categories of behaviours, such as attacking, anogenital inspection, rump presentation, mounting, and receiving and giving grooming during the social test (Extended Data Fig. 6g–l). The aggregate social behaviour values decreased in the subsequent five minutes for the control group, and approached that of the mutant monkeys (Extended Data Fig. 6m). Analysing the behaviours of the wild-type probe monkeys (that is, the monkeys with which the mutant and control groups interacted) during the same time period revealed notable differences between pairings with wild-type controls and the *SHANK3* mutants. In aggregate measures, the probe monkeys

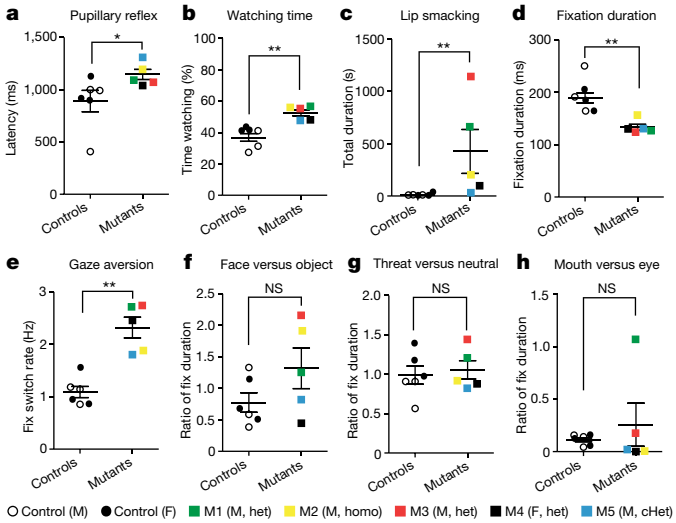

Fig. 4 | Eye-tracking properties in *SHANK3*-mutant macaques. **a**, Latency of pupillary reflex upon stimuli illuminance is increased in *SHANK3* mutants. **b**, Percentage of time watching the screen is increased in *SHANK3* mutants. **c**, *SHANK3* mutants display increased lip smacking when watching the video presentation of close-up and whole-body videos of monkeys. **d**, The duration of each fixation during the presentation of images was reduced in *SHANK3* mutants. **e**, Increased fixation-switch rate in *SHANK3* mutants. **f**–**h**, No difference in the ratio of fixation duration in face versus object (**f**), threat versus neutral faces (**g**) or mouth versus eye region (**h**) from macaques tested with image stimuli. NS, not significant. $n = 6$ macaques for control group; $n = 5$ macaques for mutant group. $P = 0.0303$ (**a**), 0.0043 (**b**), 0.0043 (**c**), 0.008 (**d**) and 0.0043 (**e**). Data are presented as mean ± s.e.m. Two-tailed Mann–Whitney *U*-test. Coloured squares indicate individual monkeys with *SHANK3* mutation.

spent less time playing with the *SHANK3* mutants than they did playing with the controls (Fig. 3e, Extended Data Fig. 7a–k). The differential effects on probe monkeys are reminiscent of the effects of oxytocin and vasopressin application on looking behaviour in macaques[29]. These results suggest the *SHANK3*-mutant monkeys display reduced levels of exploration, social interaction and vocalization, which seem to parallel some aspects of the phenotypes that are found in humans with Phelan–McDermid syndrome or autism spectrum disorder.

Altered gaze properties

We designed a video-based eye-tracking assay to investigate differences in gaze between control and mutant monkeys[30,31]. The mutants showed an increased latency of pupillary reflex to the onset of luminance at the start of the video stimulus (Fig. 4a), which is consistent with previous reports of delayed pupil reflex in humans with autism spectrum disorder[32]. The mutant monkeys spent more time watching both social and non-social videos than did controls (Fig. 4b). However, during the presentation of close-up and whole-body videos, mutant monkeys displayed frequent lip smacking and teeth chattering, which could be an indication of increased levels of anxiety or fear in response to the appearance of a conspecific[33,34] (Fig. 4c). We also assessed eye movements while the monkeys viewed pairwise still images of macaque faces and objects, or faces with threating and neutral expression[35,36]. Across all images, the mean dwell time per fixation was reduced in the mutant group (Fig. 4d). There was an increased rate of switching fixations between the two images (Fig. 4e), but not in the ratio of total fixation time (Fig. 4f–h). It has also previously been shown that human children who later develop autism have shorter durations of fixation[37].

To evaluate the cognitive performance of mutant monkeys, we trained them to perform a visual discrimination task, a reversal task and a Hamilton search task[18]. Despite extensive training, mutants M2 and M5 failed to participate in the test—possibly owing to impaired motor coordination or cognitive deficits. In black–white discrimination and reversal tasks, the controls and remaining mutants (M1, M3 and M4) performed similarly (Extended Data Fig. 8). In a Hamilton search task with three phases (Extended Data Fig. 9a), mutant and control monkeys were similar in first phase. However, M3 did not improve in the second phase (Extended Data Fig. 9b) and in the third phase, M1 and M4 exhibited learning impairment (Extended Data Fig. 9c). A χ^2 test of the proportion of monkeys that met a criterion of being correct 75% of the time by the final day of testing revealed a difference between the six controls and three mutants (Extended Data Fig. 9d). These results suggest a possible impairment in the mutants in terms of their switching strategies across the phases of Hamilton search; however, the small number of mutant monkeys that could perform the task prevent us from reaching a firm conclusion regarding the nature of their impairment.

Altered brain connectivity

MRI studies of individuals with autism spectrum disorder suggest that considerable structural and functional changes of the brain are associated with this disorder[38,39]. Structural MRI analysis in *SHANK3*-mutant monkeys revealed a decrease in grey matter but no difference in white matter and cerebrospinal fluid volumes, compared to those of controls (Extended Data Fig. 10a–c).

Altered functional connectivity has recently emerged as a possible biomarker for autism spectrum disorder[40–42]. We used an unbiased, data-driven, voxel-by-voxel, global and local functional correlation[43] (see Methods), and found that long-range connectivity between several brain regions in mutants was reduced relative to that in controls. Notably, we found that in mutants there was hypo-connectivity in putative default-mode networks, including the posterior cingulate cortex, medial prefrontal region and motor regions (Fig. 5a, d–f). We also identified local hypo-connectivity in thalamic and striatal regions (Fig. 5b, c, g, h) in the mutants. By contrast, we detected local hyper-connectivity in the somatosensory cortex, extrastriate cortical areas, and posterior cingulate cortex of the mutant monkeys (Fig. 5b, c, i, j). Seed-based analysis confirmed these results of reduced global connectivity and greater local connectivity in *SHANK3* mutants (Extended Data Fig. 10d–f). Taken together, our MRI data indicate that the mutant macaques have a dysregulated resting-state connectivity, both globally and locally.

Discussion

In this model of the *SHANK3* mutation in macaques, we observed a combination of reduced mobility, increased repetitive behaviours and impaired sociability that reconciles previous studies in rodents[2,11,26,27]. *SHANK3* mutants exhibit notable sleep disturbances and activity differences, which may assist in the discovery of characteristic biomarkers for Phelan–McDermid syndrome, autism spectrum disorder and other neurodevelopmental disorders in humans[38,44]. Altered social behaviours and stereotypy (such as licking fingers and cage bars), as well as reduced muscle strength and a lack of vocalization, in the *SHANK3*-mutant monkeys parallels the hypotonia and speech or language impairments of children with autism spectrum disorder or Phelan–McDermid syndrome[4,8]. An altered pupillary light reflex, such as we found in the mutant monkeys, has been reported in autism spectrum disorder[32]; this has not specifically been examined in Phelan–McDermid syndrome, and warrants further exploration. *SHANK3* mutants displayed comparable learning ability to controls in a simple visual discrimination task. However, a more-complex Hamilton search task revealed learning impairments that might arise from reduced flexibility or switching of strategies. Given that we could behaviourally test only a small number of mutants, further cognitive testing of larger groups will be needed to characterize any intellectual impairment.

Autism spectrum disorder is a heterogeneous disorder both in terms of the clinical manifestation of symptoms and its underlying aetiology. In fact, the genetic predisposition for autism spectrum disorder is likely to be different among individuals, even when the same gene is affected[3–9]. It is therefore difficult to draw general conclusions from a single mutant monkey (as recently reported[24]), owing to the

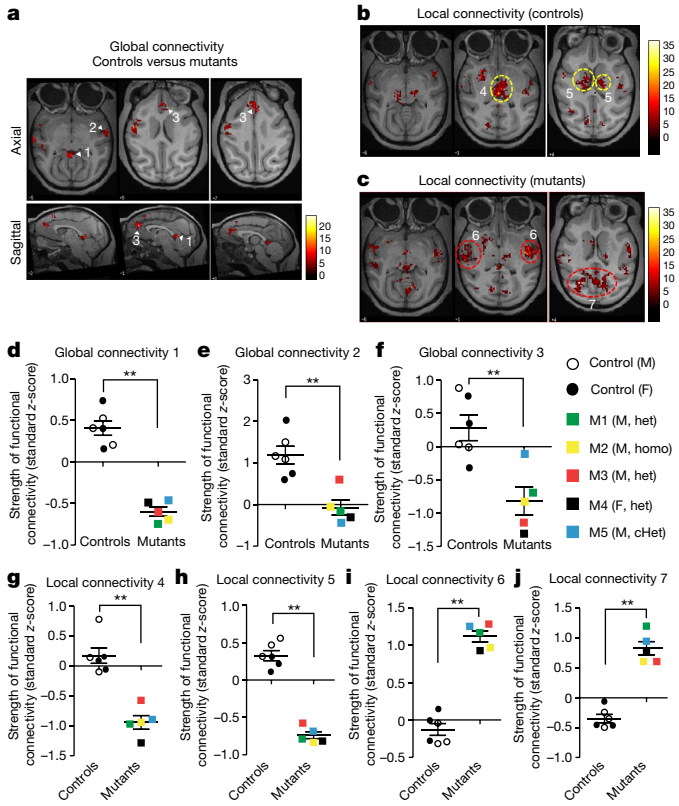

Fig. 5 | Dysregulated global and local connectivity in *SHANK3*-mutant macaques. a, Axial and sagittal views of differential global connectivity between control and mutant groups. Clusters with robustly higher global connectivity are highlighted by an arrowhead, and numbered. Putative brain regions are posterior cingulate cortex (1), motor cortex (2) and anterior cingulate cortex (3). **b**, **c**, Axial views of local connectivity in controls and mutants. Clusters with robust alteration of local connectivity are highlighted and numbered with dashed circles. Putative brain regions are thalamic regions (4), striatum (5), somatosensory cortex (6) and near the posterior cingulate cortex and extrastriate cortical areas (7). **d**–**f**, Normalized global connectivity shows a reduced strength in *SHANK3* mutants for regions 1, 2 and 3 (corresponding to **a**). **g**, **h**, Normalized local connectivity shows a reduced strength in *SHANK3* mutants for regions 4 and 5 (corresponding to **b**). **i**, **j**, Normalized local connectivity shows an increased strength in *SHANK3* mutants for regions 6 and 7 (corresponding to **c**). In **d**–**j**, $n = 6$ macaques for control group; $n = 5$ macaques for *SHANK3*-mutant group. $P = 0.0043$ (**d**), 0.0087 (**e**, **f**) and 0.0043 (**g**–**j**). Data are presented as mean ± s.e.m. Two-tailed Mann–Whitney *U*-test. Within-group threshold of $P < 0.001$ and $P < 0.05$ family-wise error correction of $P < 0.05$ (with a cluster-forming threshold of $k > 25$) were used. Coloured squares indicate individual monkeys with *SHANK3* mutation.

heterogeneity of symptoms that are related to this disorder, as well as the variability of personalities and abilities even in wild-type monkeys. Among the five founder *SHANK3*-mutant macaques, we observed considerable heterogeneity in the severity of behavioural manifestations, including motor impairments, stereotypies and learning problems in a complex task. Differential behavioural outcomes could result from normal inter-monkey variability, different mutation patterns in *SHANK3* and/or different genetic backgrounds owing to the monkeys being outbred. Among the five mutant monkeys, M4 is closer to the wild-type controls than are the other mutants for many behavioural variables (for example, total activity measure; Fig. 2g), which is consistent with its genotype and protein expression. M4 carries an in-frame deletion that causes a reduction in the levels of SHANK3 protein of about 20%; the level of reduction in SHANK3 protein isoforms is greater in the homozygous mutant (M2), the compound-heterozygous mutants (M1 and M5) and the heterozygous mutant (M3). Given the small number of monkeys in this study, as well as their genetic heterogeneity, all of our findings will need to be confirmed in larger numbers of monkeys in the future. Some of the genetic heterogeneity will be better controlled in F1-generation macaques.

In this initial characterization of *SHANK3* mutants, we are unable to pinpoint any of the causes that might underlie the behavioural differences. Anxiety disorder, exacerbated in a social context, could be a common contributor[45,46]. The hypoactivity and compromised general exploratory activity that we observed in *SHANK3*-mutant monkeys could contribute to the low reciprocity of social interactions and lack of vocalization, although the movement velocity of the mutants during the social tests did not differ from that of the controls. The altered structural MRI and neural connectivity measures may be immune to possible confounding factors. Clinical studies have shown that children and adults with sleep disorders are prone to develop language problems, and have compromised attention and executive function compared to healthy sleepers[44]. Autistic children with serious sleep disorders may have difficulty controlling repetitive behaviours, and may show a lower performance on tests of attention and memory[47]. The *SHANK3*-mutant monkeys provide an opportunity to test complex interactions such as these in the future.

Autism spectrum disorder is thought to affect multiple interconnected regions of the brain, and there is evidence for alterations in brain connectivity that could contribute to the behavioural phenotypes that are associated with autism spectrum disorder[39,48]. Recent studies have suggested that non-human primates have a resting-state default-mode network that is similar to that of humans[49,50]. Our discovery in a non-human-primate model of atypical connectivity in local and long-range circuits—especially in the cingulate, frontal, thalamic and striatal regions—suggests a path for further studies to identify circuit abnormalities and potential biomarkers for treatment studies. Monogenic forms of autism spectrum disorder may also offer insights into altered functional brain connectivity in polygenic or idiopathic autism spectrum disorder. Future longitudinal studies of resting-state functional connectivity, combined with in vivo recordings and circuit manipulations, in the second generation of *SHANK3*-mutant monkeys may allow for an in-depth understanding of the development of aberrant connectivity in neural circuits and their relevance for the behavioural phenotypes that characterize autism spectrum disorder.

Online content

Any methods, additional references, Nature Research reporting summaries, source data, statements of data availability and associated accession codes are available at https://doi.org/10.1038/s41586-019-1278-0.

Received: 4 November 2018; Accepted: 13 May 2019;
Published online: 12 June 2019

1. Naisbitt, S. et al. Shank, a novel family of postsynaptic density proteins that binds to the NMDA receptor/PSD-95/GKAP complex and cortactin. *Neuron* **23**, 569–582 (1999).
2. Jiang, Y. H. & Ehlers, M. D. Modeling autism by *SHANK* gene mutations in mice. *Neuron* **78**, 8–27 (2013).
3. Moessner, R. et al. Contribution of *SHANK3* mutations to autism spectrum disorder. *Am. J. Hum. Genet.* **81**, 1289–1297 (2007).
4. Phelan, K. & McDermid, H. E. The 22q13.3 deletion syndrome (Phelan–McDermid Syndrome). *Mol. Syndromol.* **2**, 186–201 (2012).
5. Betancur, C. & Buxbaum, J. D. SHANK3 haploinsufficiency: a "common" but underdiagnosed highly penetrant monogenic cause of autism spectrum disorders. *Mol. Autism* **4**, 17 (2013).
6. Sanders, S. J. et al. Insights into autism spectrum disorder genomic architecture and biology from 71 risk loci. *Neuron* **87**, 1215–1233 (2015).
7. Leblond, C. S. et al. Meta-analysis of SHANK mutations in autism spectrum disorders: a gradient of severity in cognitive impairments. *PLoS Genet.* **10**, e1004580 (2014).
8. Frank, Y. et al. A prospective study of neurological abnormalities in Phelan–McDermid syndrome. *J. Rare Disord.* **5**, 1–13 (2017).
9. Chen, J. A., Peñagarikano, O., Belgard, T. G., Swarup, V. & Geschwind, D. H. The emerging picture of autism spectrum disorder: genetics and pathology. *Annu. Rev. Pathol.* **10**, 111–144 (2015).
10. Gauthier, J. et al. De novo mutations in the gene encoding the synaptic scaffolding protein *SHANK3* in patients ascertained for schizophrenia. *Proc. Natl Acad. Sci. USA* **107**, 7863–7868 (2010).

11. Peça, J. et al. *Shank3* mutant mice display autistic-like behaviours and striatal dysfunction. *Nature* **472**, 437–442 (2011).
12. Jennings, C. G. et al. Opportunities and challenges in modeling human brain disorders in transgenic primates. *Nat. Neurosci.* **19**, 1123–1130 (2016).
13. Bauman, M. D. & Schumann, C. M. Advances in nonhuman primate models of autism: integrating neuroscience and behavior. *Exp. Neurol.* **299**, 252–265 (2018).
14. Chang, S. W. et al. Neuroethology of primate social behavior. *Proc. Natl Acad. Sci. USA* **110**, 10387–10394 (2013).
15. Platt, M. L., Seyfarth, R. M. & Cheney, D. L. Adaptations for social cognition in the primate brain. *Phil. Trans. R. Soc. Lond. B* **371**, 20150096 (2016).
16. Izpisua Belmonte, J. C. et al. Brains, genes, and primates. *Neuron* **86**, 617–631 (2015).
17. Sclafani, V. et al. Early predictors of impaired social functioning in male rhesus macaques (*Macaca mulatta*). *PLoS ONE* **11**, e0165401 (2016).
18. Liu, Z. et al. Autism-like behaviours and germline transmission in transgenic monkeys overexpressing MeCP2. *Nature* **530**, 98–102 (2016).
19. Chen, Y. et al. Modeling Rett syndrome using TALEN-edited MECP2 mutant cynomolgus monkeys. *Cell* **169**, 945–955 (2017).
20. Sasaki, E. et al. Generation of transgenic non-human primates with germline transmission. *Nature* **459**, 523–527 (2009).
21. Cong, L. et al. Multiplex genome engineering using CRISPR/Cas systems. *Science* **339**, 819–823 (2013).
22. Niu, Y. et al. Generation of gene-modified cynomolgus monkey via Cas9/RNA-mediated gene targeting in one-cell embryos. *Cell* **156**, 836–843 (2014).
23. Zhao, H. et al. Altered neurogenesis and disrupted expression of synaptic proteins in prefrontal cortex of *SHANK3*-deficient non-human primate. *Cell Res.* **27**, 1293–1297 (2017).
24. Tu, Z. et al. CRISPR/Cas9-mediated disruption of *SHANK3* in monkey leads to drug-treatable autism-like symptoms. *Hum. Mol. Genet.* **28**, 561–571 (2019).
25. Durand, C. M. et al. Mutations in the gene encoding the synaptic scaffolding protein SHANK3 are associated with autism spectrum disorders. *Nat. Genet.* **39**, 25–27 (2007).
26. Zhou, Y. et al. Mice with *Shank3* mutations associated with ASD and schizophrenia display both shared and distinct defects. *Neuron* **89**, 147–162 (2016).
27. Speed, H. E. et al. Autism-associated insertion mutation (InsG) of *Shank3* exon 21 causes impaired synaptic transmission and behavioral deficits. *J. Neurosci.* **35**, 9648–9665 (2015).
28. Bae, S., Park, J. & Kim, J. S. Cas-OFFinder: a fast and versatile algorithm that searches for potential off-target sites of Cas9 RNA-guided endonucleases. *Bioinformatics* **30**, 1473–1475 (2014).
29. Jiang, Y. & Platt, M. L. Oxytocin and vasopressin flatten dominance hierarchy and enhance behavioral synchrony in part via anterior cingulate cortex. *Sci. Rep.* **8**, 8201 (2018).
30. Falck-Ytter, T., Bölte, S. & Gredebäck, G. Eye tracking in early autism research. *J. Neurodev. Disord.* **5**, 28 (2013).
31. Mosher, C. P., Zimmerman, P. E. & Gothard, K. M. Videos of conspecifics elicit interactive looking patterns and facial expressions in monkeys. *Behav. Neurosci.* **125**, 639–652 (2011).
32. Daluwatte, C. et al. Atypical pupillary light reflex and heart rate variability in children with autism spectrum disorder. *J. Autism Dev. Disord.* **43**, 1910–1925 (2013).
33. Maestripieri, D. & Wallen, K. T. Affiliative and submissive communication in rhesus macaques. *Primates* **38**, 127–138 (1997).
34. Hinde, R. A. & Rowell, T. E. Communication by postures and facial expressions in the rhesus monkey (*Macaca mulatta*). *J. Zool.* **138**, 1–21 (1962).
35. Gothard, K. M., Battaglia, F. P., Erickson, C. A., Spitler, K. M. & Amaral, D. G. Neural responses to facial expression and face identity in the monkey amygdala. *J. Neurophysiol.* **97**, 1671–1683 (2007).
36. Parr, L. A. & Heintz, M. Facial expression recognition in rhesus monkeys, *Macaca mulatta*. *Anim. Behav.* **77**, 1507–1513 (2009).
37. Wass, S. V. et al. Shorter spontaneous fixation durations in infants with later emerging autism. *Sci. Rep.* **5**, 8284 (2015).
38. Tabet, A. C. et al. A framework to identify contributing genes in patients with Phelan–McDermid syndrome. *NPJ Genom. Med.* **2**, 32 (2017).
39. Rudie, J. D. et al. Altered functional and structural brain network organization in autism. *Neuroimage Clin.* **2**, 79–94 (2013).
40. Emerson, R. W. et al. Functional neuroimaging of high-risk 6-month-old infants predicts a diagnosis of autism at 24 months of age. *Sci. Transl. Med.* **9**, eaag2882 (2017).
41. Lewis, J. D., Theilmann, R. J., Townsend, J. & Evans, A. C. Network efficiency in autism spectrum disorder and its relation to brain overgrowth. *Front. Hum. Neurosci.* **7**, 845 (2013).
42. Buckner, R. L., Andrews-Hanna, J. R. & Schacter, D. L. The brain's default network: anatomy, function, and relevance to disease. *Ann. NY Acad. Sci.* **1124**, 1–38 (2008).
43. Whitfield-Gabrieli, S. & Nieto-Castanon, A. Conn: a functional connectivity toolbox for correlated and anticorrelated brain networks. *Brain Connect.* **2**, 125–141 (2012).
44. Goldman, S. E. et al. Defining the sleep phenotype in children with autism. *Dev. Neuropsychol.* **34**, 560–573 (2009).
45. Adolphs, R. The social brain: neural basis of social knowledge. *Annu. Rev. Psychol.* **60**, 693–716 (2009).
46. Arnsten, A. F. Stress signalling pathways that impair prefrontal cortex structure and function. *Nat. Rev. Neurosci.* **10**, 410–422 (2009).
47. Guénolé, F. et al. Melatonin for disordered sleep in individuals with autism spectrum disorders: systematic review and discussion. *Sleep Med. Rev.* **15**, 379–387 (2011).
48. Just, M. A., Keller, T. A., Malave, V. L., Kana, R. K. & Varma, S. Autism as a neural systems disorder: a theory of frontal-posterior underconnectivity. *Neurosci. Biobehav. Rev.* **36**, 1292–1313 (2012).
49. Moeller, S., Nallasamy, N., Tsao, D. Y. & Freiwald, W. A. Functional connectivity of the macaque brain across stimulus and arousal states. *J. Neurosci.* **29**, 5897–5909 (2009).
50. Vincent, J. L. et al. Intrinsic functional architecture in the anaesthetized monkey brain. *Nature* **447**, 83–86 (2007).

Acknowledgements We thank L. Harp McGovern and the late P. J. McGovern for their vision and support; F. Zhang for advice and reagents for CRISPR; D. G. Amaral for sharing image resources for creating eye-tracking stimuli; J. Bachevalier for advice on behavior testing; E. A. Murray for guidance on the Wisconsin General Test Apparatus assay; G. Genovese and R. Rosario for support with statistical and bioinformatics analysis; S. Sharma, S. Lall and S. Krol for critical reading of the manuscript; L. Dennis, N. Nien-Chu Espinoza, S. Yang, A. Chakrabarti, N. Joshi and Y. Fukumura for behavioral scoring; X. Wu, X. Ding, L. Cheng and X. Liu for technical support; the veterinary team of Blooming-Spring for excellent colony management and technical support; and S. E. Hyman (Stanley Center for Psychiatric Research, Broad Institute of MIT and Harvard), N. Sanjana (NYU) and L. Cong (Stanford University) and members of the Feng laboratory at MIT for critical discussion on this project. This work was supported by National Key R&D Program of China (2017YFC1307500); Shenzhen Overseas Innovation Team Project (KQTD20140630180249366); Guangdong Innovative and Entrepreneurial Research Team Program (2014ZT05S020). S.Y. and Q.K. was supported by Frontier and Innovation of Key Technology Project in Science and Technology Department of Guangdong Province (2014B020225007 and 2019B020235002); and Program for New Century Excellent Talents in University of Ministry of Education of the People's Republic of China (NCET-12-1078). This work was also supported by the National Key R&D Program of China (2018YFA0107203 and 2017YFA0103802 to A.P.X., 2017YFA0103802 to W.L.); the External Cooperation Program of Chinese Academy of Sciences (172644KYSB20160026); International Partnership Program of Chinese Academy of Sciences (172644KYS820170004 to L.W., 172644KYSB20160175 to H.Z.); the Patrick J. McGovern Foundation; Hundred Talent Program of Chinese Academy of Sciences to H.Z.; the National Natural Science Foundation of China (81425016 to A.P.X., 31671119 to Z.L.); Shenzhen Science and Technology Innovation Commission grants (JCYJ20151030140325151 to H.Z.; GJHZ20160229200136090, JCYJ20170413165053031 to T.Y.; JCYJ20170413162938668 to Z.L.). Y. Zhou was supported by postdoctoral fellowships from the Simons Center for the Social Brain at MIT and Nancy Lurie Marks Family Foundation. G.F. is supported by the McGovern Institute for Brain Research at MIT, James and Patricia Poitras Center for Psychiatric Disorders Research at MIT, the Stanley Center for Psychiatric Research at the Broad Institute of MIT and Harvard, the Hock E. Tan and K. Lisa Yang Center for Autism Research at MIT, and Edward and Kay Poitras. L.W. is also supported by Guangdong Provincial Key Laboratory of Brain Connectome and Behavior 2017B030301017, Shenzhen Discipline Construction Project for Neurobiology DRCSM [2016]1379, and Shenzhen-Hong Kong Institute of Brain Science.

Reviewer information *Nature* thanks Thomas Bourgeron, Michael Platt and the other anonymous reviewer(s) for their contribution to the peer review of this work.

Author contributions G.F., S.Y. and Y. Zhou conceived the study, and R.D., G.F. and H.Z. provided ongoing guidance on the design. S.Y. and A.P.X. oversaw the generation of mutant monkeys. H.Z. oversaw the characterization of mutant monkeys. Y. Zhou carried out CRISPR design and validation. S.Y., Q.K., H.C., Y. Zhou, J.Y., D.X., Y.H. and A.P.X. generated mutant monkeys. Y. Zhou and D.W. designed and performed molecular, protein, sequencing and off-target analyses. R.L., J.S., Y. Zhou, G.F. and R.D. designed and analysed behavioural experiments and MRI assays. H.Z., L.W., Z.L., T.Y., Y. Zou, M.J., W.J., Y.B., W.M., T.A., Y.L., X.L., W.L., L.H., S.A.A. and M.S. participated in the design or execution of some of the behavioural experiments. R.L., D.S.H., J.W.F. III, J.B.H., A.F.-K., O.M. and S.P. managed and performed behavioural scoring. Y. Zhou, R.L., R.D., J.S. and G.F. wrote the manuscript with input from all authors.

Competing interests The authors declare no competing interests.

Additional information

Extended data is available for this paper at https://doi.org/10.1038/s41586-019-1278-0.

Supplementary information is available for this paper at https://doi.org/10.1038/s41586-019-1278-0.

Reprints and permissions information is available at http://www.nature.com/reprints.

Correspondence and requests for materials should be addressed to H.Z., A.P.X., G.F. or S.Y.

Publisher's note: Springer Nature remains neutral with regard to jurisdictional claims in published maps and institutional affiliations.

METHODS

CRISPR construct, cell culture and mRNA preparation. Selected gRNAs that target exon 21 of macaque *SHANK3* were cloned into the pU6-gRNA expression plasmid separately, using the two BbsI restriction sites. Sequence-verified gRNA-expressing plasmids were individually co-electroporated into primary cultured fibroblast cells together with wild-type *Sp*Cas9-expressing plasmid (Primate Biologicals) and cultured for 48 h using dermal fibroblast culture medium (Zenbio). Cells were collected, and total genomic DNA was extracted using a NucleoSpin tissue kit (Macherey-Nagel). An amplicon of 700 bp flanking the targeted mutation region of *SHANK3* was amplified from each DNA sample, followed by analysis using a standard surveyor nuclease-based mutation detection assay as described in the user manual (IDTDNA). To prepare CRISPR mRNAs for embryo injection, guide RNA no. 1 and no.2, and wild-type *Sp*Cas9-expressing plasmid, were linearized and transcribed with commercial kits (MEGAscript T7 (Ambion) and HiScribe T7 (NEB)). Synthesized mRNA was further purified with MEGAclear Transcription clean-up kit (Ambion) and quantified with Nanodrop 2000 (Thermo Fisher). Monkey embryos injected with *SHANK3* CRISPR mRNA were cultured for 5 to 7 days and collected individually, lysed with protease K; this was followed by nested PCR-based genotyping of 300-bp amplicons using two sets of primers. Primer set I forward: 5′-gacccctgtttgtggatgtacagg-3′; reverse: 5′-cctggcccggggt ctgctggggtgccgc-3′; primer set II forward: 5′-ggtccctggcttccccggccttctcc-3′; reverse: 5′-gctgggcaggggctctgccacagctgc-3′. The presence of indels in the injected embryos was revealed by electrophoresis-based separation on 4% agarose gel and subsequent Sanger sequencing of the PCR product.

Genotyping of mutant monkeys and off-target analysis. To genotype *SHANK3* mutation in newborn macaques, a 1-kb PCR product flanking the desired mutation site was amplified using high-fidelity polymerase (PrimeSTAR HS DNA Polymerase with GC buffer) from genomic DNA of each monkey, using primer forward: 5′-atcgaattcgctccactgtgttcctgtccgt-3′ and reverse: 5′-tacggatccatggtgcttgt-ggtctccaggtgggggtc-3′. PCR products from individual monkeys were cloned separately into pBSKII vector using the EcoRI and BamHI restriction sites. Ligation mixtures were transformed into competent *Escherichia coli* and plated onto plates with ampicillin selectivity. Individual bacterial colonies were picked up, and plasmid DNA was subjected to Sanger sequencing to examine various types of indels and their percentages. Possible off-target sites caused by administration of single-guide (sg)RNA1- and sgRNA2-guided Cas9 endonucleases for exon 21 of *SHANK3* gene were predicted by scanning Macaca_fascicularis_5.0 of the UCSC genome database through Cas-OFFinder, a bioinformatics-based algorithm (http://www.rgenome.net/cas-offinder/). Genomic DNA from peripheral whole blood from all five *SHANK3* mutants and two wild-type monkeys was extracted and used for subsequent analysis. The top ten predicted off-target sites ranging from one to three mismatches within targeted sequences of each sgRNA were amplified by a high-fidelity polymerase. Purified PCR products of each predicted site from individual monkeys were aligned and examined using Sanger sequencing. Detailed annotation of all predicted off-target sites, primers used for PCR amplification and summary of sequencing results are available in Supplementary Table 1.

Craniotomy and brain biopsy. Surgical procedures were performed after completing all behavioural analysis and MRI scanning presented in this study. While the monkeys were under general anaesthesia, a craniotomy was performed and a 2-mg biopsy was taken from the surface of V1.

Western blotting and semi-quantification of protein expression. Biopsy samples from the superficial V1 layer of each monkey were briefly sonicated inside 100 μl of PBS solution containing protease inhibitor (Roche). A sonication protocol consisting of 10% power and three pulses with 30% on and 70% off (Omni-Ruptor 250) was carried out to ensure complete lysis of tissue sample. After quantification with BCA kit (Pierce), the calculated amount of each protein was mixed with an equivalent amount of 2× Laemmli sample buffer (Bio-Rad) and boiled for 5 min at 95 °C. Sample volumes corresponding to 20 μg of total protein amount per lane were loaded onto 4–15%-gradient Mini-PROTEAN TGX gels (Bio-Rad) and ran for 3 h at 60 V. The proteins were then transferred onto Whatman Protran nitrocellulose membranes (0.2-μm pore size, BA83, Sigma Aldrich) using a tank blot system (Mini Trans-Blot Cell, Bio-Rad) for 120 min at 100 V at 4 °C. The membranes were blocked for 1 h with 5% non-fat milk dissolved in TBS buffer that did not contain any Tween-20. Subsequently, the membranes were incubated with primary antibodies diluted in Odyssey blocking buffer (Li-COR Biosciences) with a dilution factor of 1:100 for N-terminal SHANK3 antibody (NIH NeuroMab N367/62) and 1:500 for C-terminal SHANK3 antibody (Santa Cruz Biotech SC-30193) for 12 h at 4 °C. Following primary antibody incubation, the membranes were washed 3 times for 5 min per wash using TBST buffer (0.05% Tween-20). Then, the secondary antibodies, goat-anti-mouse IRDye 680 (Li-COR Biosciences), donkey-anti-rabbit IRDye 800CW (Li-COR Biosciences) diluted in 1:1 TBST (0.05% Tween-20):Odyssey Blocking Buffer (Li-COR Biosciences), were incubated with the membrane for 1 h at room temperature. Following three rounds of washing with TBST, the membranes were scanned using an Odyssey CLx infrared imaging system (Li-COR Biosciences). Specific bands were then quantified with the contrast-independent, automatic background-subtraction rectangular region-of-interest (ROI) tool of the built-in Software Image Studio 3.1 (Li-COR Biosciences), and normalized to an α-tubulin loading control for each lane and each blot. The values obtained for each sample from mutant monkeys were then normalized to the wild-type expression. To estimate the percentile of remaining isoforms of the SHANK3 protein, five technical repeats of western blot using the same protein lysis were analysed and averaged values for each mutant monkey were presented.

Statement on animal work. All animal-related work was done in accordance with NIH guide for the care and use of laboratory animals (https://www.ncbi.nlm.nih.gov/books/NBK54050/) and institutional animal care and use guidelines approved by the IACUC of Shenzhen Institutes of Advanced Technology, Chinese Academy of Sciences. We also followed nc3r recommendations (https://www.nc3rs.org.uk/) by using the minimum number of mutants and age-matched controls, while maintaining statistical reliability. The cynomolgus monkey (*M. fascicularis*) breeding facilities, housing and primate laboratories used in this study are accredited by The Association for Assessment and Accreditation of Laboratory Animal Care. Wild-type and mutant monkeys in the experimental groups were housed in an environmentally controlled facility (temperature: 22 ± 1 °C, humidity: 50 ± 5% relative humidity) with 12-h light/12-h dark cycle (lights on at 07:00). All macaques were fed with commercial monkey diet twice per day, plus one meal of seasonal fruits daily, and with free access to a water bottle. Monkeys were under careful veterinary monitoring twice per day to evaluate and ensure their health status. Infant monkeys were housed with their mothers and weaned at 12 months of age. After weaning, pairs of young monkeys were selected for compatibility and pair-housed together in both the wild-type control group and the *SHANK3*-mutant group. The pairing strategy for the mutant group was: M1 with M3, and M2 with M5; the female mutant M4 was paired with a female from the control group. A sliding divider was used to temporarily separate two monkeys during certain procedures, including video recording of home-cage activity, the wearing of motion watches and recovery from anaesthesia or surgical procedures.

Surgical procedures and generation of *SHANK3*-mutant monkeys. Detailed procedures related to superovulation, oocytes collection, intracytoplasmic sperm injection (ICSI), CRISPR injection, embryo transfer, and pregnancy diagnosis are documented as previously reported[51]. In brief, female cynomolgus monkeys aged 7–12 years with regular menstrual cycles were chosen as oocyte donors for superovulation and recipients for embryo transfer after genetic engineering. Healthy male monkeys aged 5–10 years of proven fertility were chosen as sperm donors. Under general anaesthesia, laparoscopic procedures were performed aseptically for both oocyte collection and embryo transfer in females. Female monkeys were intramuscularly injected with recombinant human FSH (rhFSH) (EMD Serono) twice per day consecutively for eight days, followed by one injection of recombinant human chorionic gonadotropin (rhCG) (EMD Serono) on day 9. Oocytes were collected through laparoscopic-guided follicular aspiration 33–36 h after administration of rhCG. Mature oocytes at stage MII were selected to perform fertilization using ICSI. Seven-to-eight hours after sperm injection, embryos with the clear appearance of two pronuclei were injected into cytoplasm with a mixture of mRNAs containing 50 ng/μl of *Sp*Cas9, 25 ng/μl of gRNA 1 and 25 ng/μl of gRNA 2. Injected embryos were immediately transferred into the oviduct of the stage-matched recipient female monkeys. Successful implantation of embryos and pregnancy of recipient were examined by ultrasonography four weeks after embryo transfer.

Data analysis and statistical comparisons. All behavioural observations, scoring, data analysis in this study were carried out by trained observers without previous knowledge of the experimental design and goal of this study. All data are presented as mean ± s.e.m. Comparisons between *SHANK3*-mutant monkeys and the wild-type control group were analysed using a nonparametric, two-tailed Mann–Whitney *U*-test, unless otherwise specified in the legend of each figure (GraphPad Prism 5). $*P < 0.05$; $**P < 0.01$; $***P < 0.001$. Statistical power was calculated using the following steps. First, statistical tests were run on the control and mutant measurements; sample means and standard deviations were then calculated; Cohen's *d* effect size from two distributions with the empirical sample means and standard deviations were then computed. Finally, simulations were run to generate a nominally significant *P* value from two distributions with the empirical sample means and standard deviations (see Supplementary Table 3 for summary of power calculations).

Activity and sleep monitoring. Activity and sleep patterns of the monkeys were recorded after suitably modifying a commercially available actigraphy device with a built-in ambient light sensor and event marker as previously described[52]. In brief, monkeys were lightly anaesthetized with ketamine, and a motion watch was placed individually. Monkeys were habituated to wear the watch for two weeks before data collection. Following habituation, daily physical activity and a full range of sleep

and circadian parameters for each monkey were recorded and collected for up to seven days. Recorded data were transferred to a host computer and analysed.

Behavioural scoring. The behaviour of the monkeys during the first year of life (starting at one month of age) was scored from video recordings (Canon, 1,920 × 1,080 at 30 frames per second) using Observer software (Noldus Observer XT 11). During this time, the monkeys were housed together with their mother. Each observer was trained by an expert observer on a subset of videos until inter-observer reliability with a highly experienced observer exceeded 0.85. After that, each observer scored a subset of the videos for data collection. Per monkey, between 12 and 49 sessions of 10 min in length each, spread throughout the year, were scored, depending on the availability of video material. The sessions were binned into periods of 16 weeks to ensure the equal contribution of periods with different sampling density to the mean for the year. We used roaming entropy to quantify the locations that animals visited in the home cage. The location of the animals in the cage was annotated as being on the left wall, right wall, floor, front wall, rear wall or ceiling, at each point in time. To quantify the evenness of the distribution of locations for each animal, entropy was calculated using the proportions of time spent in each location as previously described[53]. As an example, a monkey that spends all of its time in one location has an entropy of 0, and a monkey that spends an equal amount of time in all locations has maximum entropy, 2.585 in the present case of 6 possible locations. The coding of stereotypy of mutants included flipping, licking cage bars and licking fingers. The unit of measurement is time performing the behaviour in seconds, per minute of observation.

Habituation, social interaction and exploration. Habituation of monkeys and social interaction with other monkeys was tested in a room and cage separate from the home room and housing cage. The cage dimensions were 3 m × 1.5 m × 1.5 m (width × height × depth). Each monkey was habituated to the novel environment separately, by placing them inside the cage for 30 min on 2 separate days. A video camera was used to record the habituation and social interaction sessions. Each social interaction session consisted of the following procedure: two monkeys were taken out of their home cage, transported to the social interaction room and placed inside the cage. The monkeys were separated by a vertical divider. The divider was made of non-transparent plastic material, which blocked visual and tactile communication but not auditory and olfactory contacts between two monkeys. After approximately 10 min, the divider was removed and the monkeys could interact for 30 min. After this, the divider was re-inserted. Finally, after another 10 min, the monkeys were taken back to the home cage. Each animal in our experimental group (six controls and five mutants) went through ten social interaction sessions, during which the monkey met ten age-matched wild-type monkeys (the probe group) in random order.

Behaviour scoring during social interaction. The video material was scored for categories of behaviours, including chase, flee, follow, circle, play, attack, presentation of rump, anogenital inspection, groom and mount. The behaviours chase, follow, flee, circle and play were combined into an aggregate category labelled 'social behaviours.' We report the average total duration per 5 min for each category in the main text, and component categories in Extended Data Figs. 7, 9.

Movement tracking during habituation and social interaction. Computer vision was used to track the animals in two dimensions (x and y) during the habituation and social interaction sessions. Although actual movement occurs in three dimensions, we assume that there was enough information in the two-dimensional plane to detect potential differences between mutant and controls (see diagram in Extended Data Fig. 8f).

Tracking is performed according to the Bayesian nonparametric, linear dynamic system. $y_n^t \in R^5$ is the nth observation at time t, and denotes a (u, v, L, a, b) tuple of pixel coordinates (u, v) and colour (L, a, b). The observation model is a per-observation Gaussian mixture

$$p(y_n^t \mid z_n^t, b_n, \theta_p^t) = N(y_n^t \mid b_n, \Sigma_B)^{\mathbb{I}(z_n^t=0)} \prod_p N(y_n^t \mid \mu_p^t, \Sigma_p^t)^{\mathbb{I}(z_n^t=p)}$$

in which $\theta_p^t = (\mu_p^t, \Sigma_p^t)$ are Gaussian parameters that can be viewed conceptually as corresponding to object-part (for example, body, tail or head) locations and appearance (μ_p^t), and extents (Σ_p^t) of the objects to be tracked, and $b_n \in \mathbb{R}^5$ is a background model for the nth observation—also a (u, v, L, a, b) tuple. Part locations and appearances are generated as

$$p(\mu_p^t \mid \delta_p^t, x_k^t) = \mathrm{Unif}(\mu_p^t \mid U_X)^{\mathbb{I}(\delta_p^t=0)} \prod_k N(\mu_p^t \mid Hx_k^t, \Sigma_x)^{\mathbb{I}(\delta_p^t=k)}$$

The z_n^t variables are categorical random variables with a Griffiths–Engen–McCloskey prior; they assign observations to either background or object parts. The δ_p^t variables are also categorical random variables, but with a Dirichlet prior, as we assume a known number of targets. They assign part θ_p^t to one of K object, or to a (uniform) clutter distribution. Matrix $H = \begin{bmatrix} \mathrm{I} & 0 \\ 0 & 0 \end{bmatrix}$ projects the latent object location into the observation space. The μ_p^t and Σ_p^t components share a data-dependent normal–inverse–Wishart (NIW) prior at each time t with concentration $\frac{1}{N_p}\sum_n y_n^t$ and scale $\sum_n y_n^t (y_n^t)^{\mathrm{T}} \mathbb{I}(z_n^t = 1)$ in which $N_p = \sum_n z_n^t$ and z_n^t is a categorical random variable sampled such that $p(z_n^t = 0) \propto N(y_n^t | b_n, \Sigma_B)$ and $p(z_n^t = 1) \propto \mathrm{Unif}(y_n^t | U_\Sigma)$. Latent x_k^t variables are the independent, time-evolving image location and velocity of each tracked object with dynamics

$$p(x_k^{t+1} | x_k^t) = N(x_k^{t+1} | Ax_k^t, \Sigma_X)$$

in which $A = \begin{bmatrix} \mathrm{I} & \mathrm{I} \\ 0 & \mathrm{I} \end{bmatrix}$ enforces a random acceleration model. The inference proceeds as: for each n, estimate background model b_n as $\mathrm{median}(y_n^{1:T})$, which can be performed in $O(\log(T)\log(\log(T)))$ time with a randomized algorithm.

Then, for time $t = 1, \ldots, T$ observation $n = 1, \ldots, N$. (1) Sample $z_n^{t'}$, then estimate NIW priors for θ_p^t; (2) estimate $z_n^t, \mu_p^t, \Sigma_p^t$ using variational approximation[54]; and (3) propagate x_k^{t-1}, P_k^{t-1} to $\hat{x}_k^t, \hat{P}_k^t$ according to dynamics, then sample $\delta_p^t | \mu_p^t, x_k^t$ and compute Kalman filtered estimate $\bar{x}_k^t, \bar{P}_k^t | \{\mu_{\delta_p^t}^t : \delta_p^t = k\}$ in which $\bar{P}_k^t$ is the covariance estimate of random variable x_k^t with mean $\bar{x}_k^t$ (ref. [55]). For time $t = T, \ldots, 1$, compute smoothed estimates x_k^t via Rauch–Tung–Striebel smoothing.

Sample object trajectories can be computed as Gibbs iterations of the above, although even a single pass over the data yields good performance under reasonable conditions. Being generative, this model provides several benefits over more-standard, detection-based trackers. The output of the computer vision tracker used for the present analysis are—for each video frame—the coordinates of the centre of gravity of the pixels associated with each monkey, as well as velocity. To account for small variations in camera position and zoom level, the tracking data were normalized such that for x, 0 represents the right cage edge and 1 the left, and for y, 0 is the cage floor and 1 the top.

Location preferences. Movement during the last habituation session was analysed to determine the location preferences in control monkeys and mutants. The proportion of time spent in the left half versus the right half, and upper half versus lower half were determined using x and y location values. Here, a value of 0.5 means that the monkeys were unbiased in their exploration of locations.

Eye tracking. The eye movements of the monkeys were examined while they observed images and video clips, using a Tobii TX300 eye tracker (sampling frequency 120 Hz) under semi-freely moving conditions, without head restraint. For a subset of sessions, the monkeys were tested while in a specially designed 'eye-tracking box' with a view-port cut out. For another subgroup of sessions, the monkeys were seated in a typical primate chair. The eye tracking box is a 50-cm × 50-cm × 50-cm box made of ½-inch-thick opaque plexiglass. A 1-inch × 3-inch viewport cut out allowed the monkey to see outside (see diagram in Extended Data Fig. 8g). The monkeys were habituated to being in the box by successive exposures that increased in duration. The monkey was lured into the box with fruit. The animals received their typical diet, and were not water- or food-restricted. The eye tracker was calibrated for each monkey separately using built-in Tobii calibration routines.

Separate sessions were run with video clips as stimuli and with still images as stimuli. Video clips were played without audio. A large proportion of the video and still stimuli were created and shared by the laboratory of D. Amaral (with permission).

Video stimuli. For video sessions, 316 video clips (1,920 × 1,080 pixels) of 5–10 s in duration each were created in the following categories.

Whole body. Individual rhesus monkeys in a cage, subcategorized by emotional expression, behaving in a neutral, aggressive or submissive manner towards the camera.

Close up. Individual rhesus monkeys in a cage, behaving in a neutral, aggressive or submissive manner towards the camera. Close-ups were created by cropping original footage centred on the head and resized to 1,920 × 1,080 pixels resolution.

Group. Clips of groups of rhesus monkeys engaged in foraging, mating, grooming, aggression, play and neutral, non-social behaviour.

Miscellaneous. A mixture of 5–12-s-long clips with either abstract moving images, scenes from wildlife movies with non-primate mammalian species (farm animals, birds and dogs), children's TV shows, computer games, silent films, popular music videos and motion pictures. The 316 videos were split into three sets of 10–12 min, each containing all categories. There was a 1-s black screen interval between subsequent videos. We showed one set per session and ran one session per day. This test was repeated three times. The first time, monkeys were in the eye-tracking box. Thus, there was a total of 9 video-watching sessions with eye tracking, and each of the 316 video clips was shown 3 times.

Video eye-tracking analysis. Using Tobii Studio software, ROIs were drawn around the body, head, eyes and mouth in the whole body, close up and group videos. Eye fixations were detected using the Tobii I-VT filter at the default setting. Data were exported from Tobii studio to .csv format and analysed with custom-written MATLAB and Python scripts. The fraction of time the monkey spent watching each video clip was calculated: Fraction watched = number of samples in which the monkey was gazing within the area taken up by the video/number

of samples during which the clip was shown. In addition, the latency of pupillary light reflex to the onset of the videos was calculated. The pupil diameter was derived from every sample and averaged between left and right eye. Pupil diameter in the period between the start of each video clip, and 3.3 s into the video, was averaged across all videos for each subject. The light reflex magnitude is the difference between the diameter at $t = 0$ and the minimum diameter in the 3.3-s period. After fitting a spline to the curve, the latency of the pupillary light reflex is the point at which the diameter has reduced 0.15 of the light reflex amplitude. During some sessions, the monkey was recorded using a camcorder during eye tracking to study the animal's overt facial expressions (in particular, lip smacking). A trained observer (S.P.) annotated the video using Noldus Observer software, to determine the amount of time spent lip smacking during each video.

Still images. Still images were used in two sessions. In both, a series of images were shown, in which two photographs were shown side-by-side. The 'face versus object' session contained 44 images, each one pairing a photograph of a neutral monkey face or portrait with a photograph of plant leaves. The images of plant leaves are from the MSRC image database (http://research.microsoft.com/vision/cambridge/recognition/). In the 'neutral versus threat' session, 31 images were shown, each one pairing two portraits of the same individual monkey (one with a neutral facial expression and one with an open mouth threat expression). In both sessions, each individual monkey appeared in only one image. In most of the portraits, the monkey in them was directly looking at the camera. ROIs were drawn around the eyes and mouth, and around each picture as a whole.

Wisconsin General Test Apparatus tests. The Wisconsin General Test Apparatus (WGTA) was modelled after the original description of the apparatus[56]. The apparatus is a cage where the monkey has access to a presentation tray with four food wells, a trial door, an access door to separate the subject and presentation tray, and a camera for recording. All tests were carried out in a quiet and standardly lit room. Each trial began with opening the access door to give the monkey the chance to reach and open a food well on the presentation tray (which was counted as a response). Once a response was made, the sliding opaque door was lowered, the response was scored as correct or incorrect, and the next trial was set up. Monkeys M2 and M5 were not able to perform any of the WGTA tasks. Therefore, the data only include three mutants. To motivate the monkeys for these tasks, they were not fed before the testing session that day. Throughout the WGTA and Hamilton tasks, six wild-type monkeys from the control group and three *SHANK3*-mutant monkeys underwent the same brief fasting regime each day before their trials.

Adaptation. Before testing, the monkeys were adapted to the testing apparatus, including training to take food rewards (such as fruit) from open food wells. Once the monkeys were able to take the rewards, they were trained to displace a removable disc covering the food wells to obtain the reward. Once the monkeys were able to reliably obtain food rewards by removing objects from the food wells (23 correct out of 25 trials per day), they were trained to perform other tasks.

Black–white discrimination and reversal. Experiments were designed as previously described[57]. In this test, monkeys were required to associate a colour (a black or white block) with a food reward (discrimination phase). Once monkeys learned this association, the opposite colour was rewarded, requiring them to reverse their strategy (reversal phase). Monkeys received 25 trials per day, 5 days per week, until a set criterion for 90%-correct responses was met.

Hamilton search task. The Hamilton search task was based on previous descriptions[57,58]. In this test, a monkey sat and faced four identical wells with lids. One of the wells contained a food reward and the subject's task was to locate the food with the least number of box openings. In the first stage of the task (the 'set making' stage), the monkeys developed a search strategy to locate a food reward placed randomly in one of four wells with lids, with the exception being that the same location was never rewarded on two consecutive trials. Monkeys are required to lift the lid on the well to obtain the reward. A trial was a sequence of responses that ended with the monkey finding the food. Here the optimal solution is one in which the last well that contained food is avoided, and all other wells are opened only once. On each trial, the experimenter recorded which wells the monkey tried and in what order. The trial was terminated when the subject opened the correct well or when 60 s was up, whichever came first. The criterion was reached when the test subject successfully completed five trials in a row. Monkeys received 25 trials per day for 5 consecutive days.

In the second stage (set breaking), the well that was least-preferred in stage one was now baited on every trial, and the animal was allowed to open as many wells as necessary to locate the reward. The well that was baited did not change across trials within a test session. A perfect strategy would be to quickly discern that the same well location is always rewarded, and to only open that well on every trial. Monkeys received 25 trials per day for 5 consecutive days. We counted the number of times the monkey opened the correct well in the first try (X). For each monkey, we report the difference of X ('delta') between fifth and first day as a measure of learning.

The third stage (forced set breaking) was identical to stage two, but with a different rewarded location from stage two, and with the exception that only one well opening was allowed on every trial. The single response on that trial was marked correct or incorrect. Monkeys received 25 trials per day for 5 consecutive days. We report the percentage of correct trials for each of the five days.

Structural and functional MRI. Protocols for anaesthesia and MRI were in accordance with NIH guidelines, and were reviewed and approved by the Institutional Animal Care Committee of SIAT. In preparation for MRI scanning under anaesthesia, the monkey was premedicated with atropine (0.05 mg/kg, intramuscular) to decrease bronchial secretions, followed by ketamine (15 mg/kg, intramuscular). To prevent hypothermia, the monkey was wrapped in a blanket, the extremities were covered with mittens and were placed on a warm-water circulating blanket. The anaesthesia was maintained for the duration of the scan with intravenous propofol by continuous infusion using a syringe pump at the dose of 0.5 mg/kg/min. The anaesthetic level was adjusted to eliminate movement as assessed by toe pinches, while keeping the heart rate in the range of 100–140 beats per minute. Corneal reflexes were consistently absent. Electrocardiography, heart rate and oxygen saturation (SpO_2) (range 94–100%) were continuously monitored with an magnetic-resonance compatible monitoring system (Invivo). Rectal temperature was continuously monitored and was maintained between 37.5–38.5 °C. Magnetic resonance scanning was performed at the SIAT imaging centre on a 3T Tim Trio scanner (Siemens) using a custom-designed 8-channel radio-frequency surface head coil. Functional MRI data were acquired using a T2*-weighted gradient-echo echo-planar sequence (volume repetition time (TR) = 2.1 s, T2* echo time (TE) = 25ms, flip angle = 90°, 1.25 mm × 1.25 mm in plane resolution and slice thickness = 1.3 mm). In all monkeys, the slices were acquired using contiguous, interleaved acquisition; 128 volumes per run (3 consecutive runs, each lasting approximately 5 min) were acquired in each monkey. T1-weighted, magnetization-prepared rapid gradient echo structural images were also acquired (TR = 2.1 s; TE = 3.21 ms, flip angle = 8°, 0.5 mm isotropic voxels) and used to align the functional data to the monkey atlas as previously reported[59].

Functional MRI data analysis. Resting-state functional MRI (rsfMRI) data were first preprocessed in SPM8 (Wellcome Department of Imaging Neuroscience; www.fil.ion.ucl.ac.uk/spm), using standard spatial preprocessing steps. Data were motion-corrected, realigned, normalized to structural scans (using the monkey atlas template) and spatially smoothed with a 3-mm full-width at half maximum Gaussian kernel. The structural image of each monkey was segmented into white matter, grey matter and cerebral spinal fluid, using SPM8 as previously described[60].

Motion artefact detection. We used a standard artefact rejection toolbox (www.nitrc.org/projects/artifact_detect) for a comprehensive analysis of sources of artefacts in time-series data, including spiking and motion to identify outlier data points (TR values), defined as volumes that exceeded three z-normalized standard deviations away from mean global brain activation across the entire volume, or a composite movement threshold of 0.5 mm scan-to-scan frame-wise displacement. There was no significant difference in the number of outliers between groups. In addition, there was no significant difference in the mean or maximum head motion parameters, or the mean or maximum global signal change between groups. Maximum motion (controls 0.09 ± 0.01 versus mutants 0.099 ± 0.01; $P = 0.66$); mean motion (controls 0.036 ± 0.01; mutants 0.036 ± 0.01; $P = 0.48$).

Connectivity analysis. Functional connectivity analysis of rsfMRI data was carried out in custom software developed in MATLAB toolbox (www.nitrc.org/projects/conn/). To minimize partial volume effects with adjacent grey matter, the white matter and cerebral spinal fluid masks were eroded by one voxel and used as a noise ROI. The first three principal components of the signals from the eroded white matter and cerebral spinal fluid were regressed out through an anatomical component-based noise correction approach (aCompCor) as previously described[61]. In the aCompCor approach, segmented white matter and cerebral spinal fluid masks are eroded by one voxel to produce the white matter and cerebral spinal fluid noise ROIs. The erosion removes about 70% of the white matter voxels and 95% of the cerebral spinal fluid voxels from the original segmentations. Therefore, unlike the global signal regression approach, the white matter and cerebral spinal fluid masks used in the analysis were only a very small fraction in size, compared to the whole brain mask, which minimizes spurious correlation values. To minimize head-motion-related confounding factors, realignment parameters and their first-order derivatives, along with the motion outliers, were also regressed during de-noising. A temporal band-pass filter of 0.0025–0.05 Hz was applied to the pre-processed functional dataset. For resting-state local and global functional connectivity analysis, we used an unbiased data-driven approach instead of the standard seed-based analysis.

Integrated local correlation. Integrated local correlation (ILC) was used to assess the coupling of local neuronal processes in any given voxel's neighbourhood. The coupling of local neuronal processes influences coherence in a voxel's neighbourhood. The ILC for each voxel is an integration of its spatial correlation function. In this approach, physiological fluctuations owing to respiratory and cardiac fluctuations have minimal effect on the ILC measurement, except

perhaps in the areas that surround large blood vessels. ILC maps represent a measure of local coherence at each voxel, characterized by the average correlation between each individual voxel and a region of neighbouring voxels. Within the grey matter, ILC has previously been reported[62] to be found to be higher in the default-mode network.

Global correlation. Global correlation (GCOR) is calculated by computing the average of correlation coefficients between each individual voxel and all of the voxels in the brain. GCOR maps provide a voxel-by-voxel measurement of network centrality, characterized by the strength and sign of functional connectivity between a given voxel and every other voxel in the brain. For both ILC and GCOR, the voxel-to-voxel (local and global connectivity) measures are normalized to zero-mean, one-unit variance separately for each subject before being entered into the second-level analyses. Second-level within-group and between-group *t*-tests are performed for the ILC and GCOR maps for both controls and mutants as described in the toolbox for connectivity measures: https://sites.google.com/view/conn/measures/networks-voxel-level.

Reporting summary. Further information on research design is available in the Nature Research Reporting Summary linked to this paper.

Data availability

All data are available in the main text or the Supplementary Information. All sequencing data, images, code, and materials used in the analysis are available to researchers for the purpose of reproducing or extending the analyses.

51. Ke, Q. et al. TALEN-based generation of a cynomolgus monkey disease model for human microcephaly. *Cell Res.* **26**, 1048–1061 (2016).
52. Sri Kantha, S. & Suzuki, J. Sleep quantitation in common marmoset, cotton top tamarin and squirrel monkey by non-invasive actigraphy. *Comp. Biochem. Physiol. A* **144**, 203–210 (2006).
53. Freund, J. et al. Emergence of individuality in genetically identical mice. *Science* **340**, 756–759 (2013).
54. Bei, D. M. & Lafferty J. D. Dynamic topic models. In *Proc. 23rd International Conference Machine Learning* (2006).
55. Kalman, R. E. A new approach to linear filtering and prediction problems. *J. Basic Engineer.* **82**, 34–45 (1960).
56. Harlow, H. F. & Bromer, J. A. A test apparatus for monkeys. *Psychol. Rec.* **2**, 434–436 (1938).
57. Harlow, H. F. The development of learning in the rhesus monkey. *Am. Sci.* **47**, 459–479 (1959).
58. Levin, E. D. & Bowman, R. E. The effect of pre- or postnatal lead exposure on Hamilton Search Task in monkeys. *Neurobehav. Toxicol. Teratol.* **3**, 391–394 (1983).
59. Frey, S. et al. An MRI based average macaque monkey stereotaxic atlas and space (MNI monkey space). *Neuroimage* **55**, 1435–1442 (2011).
60. Ashburner, J. SPM: a history. *Neuroimage* **62**, 791–800 (2012).
61. Behzadi, Y., Restom, K., Liau, J. & Liu T. T. A component based noise correction method (CompCor) for BOLD and perfusion based fMRI. *Neuroimage* **37**, 90–101 (2007).
62. Deshpande, G., LaConte, S., Peltier, S. & Hu X. Integrated local correlation: a new measure of local coherence in fMRI data. *Hum. Brain Mapp.* **30**, 13–23 (2009).

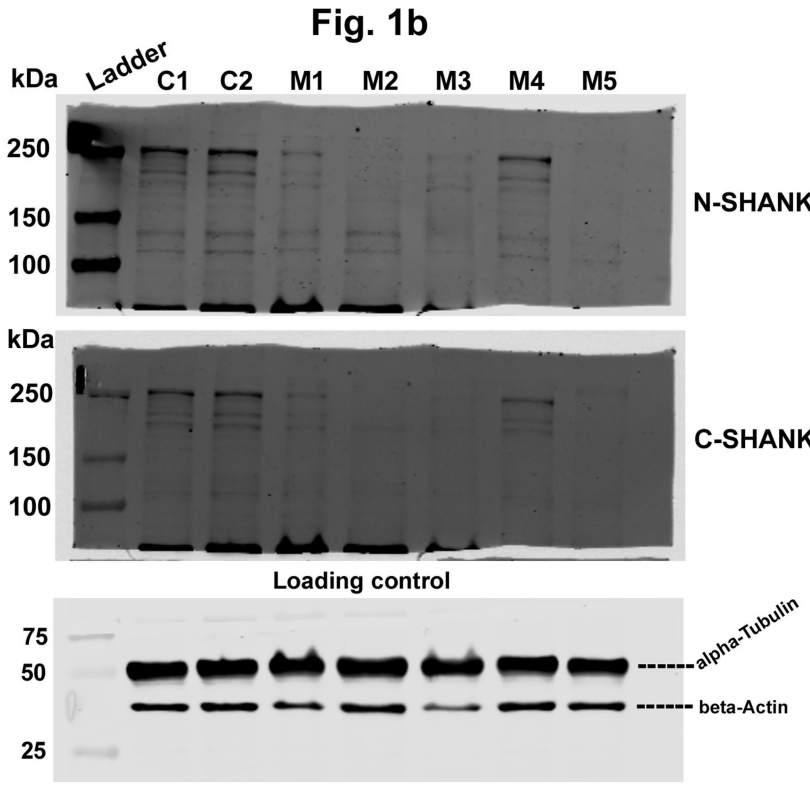

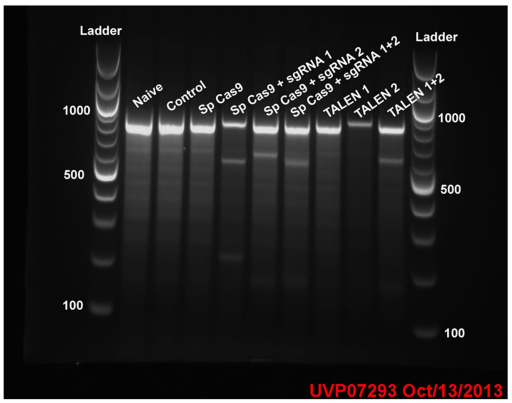

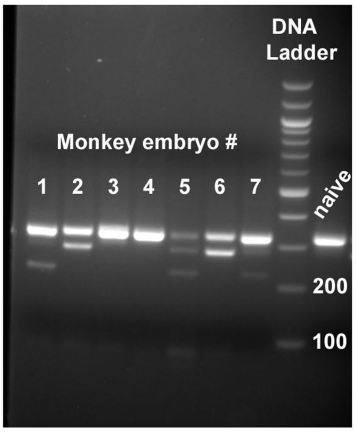

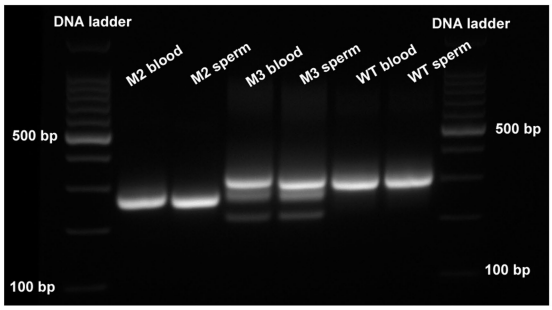

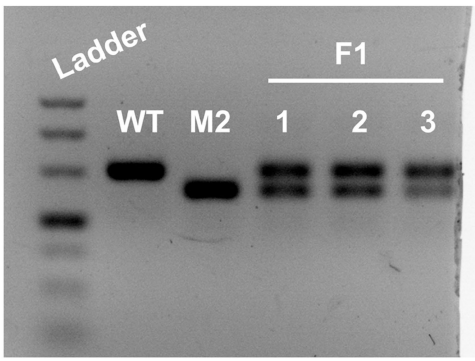

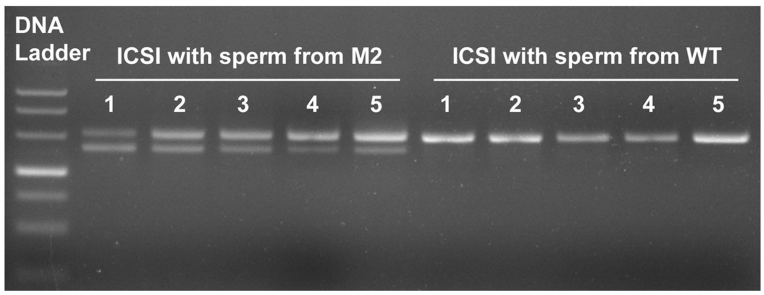

Extended Data Fig. 1 | Original images for western blots and DNA gel. Original images for western blots and DNA gel electrophoresis corresponding to specific figure panels as indicated are presented without cropping or further processing, such as adjusting of brightness and contrast.

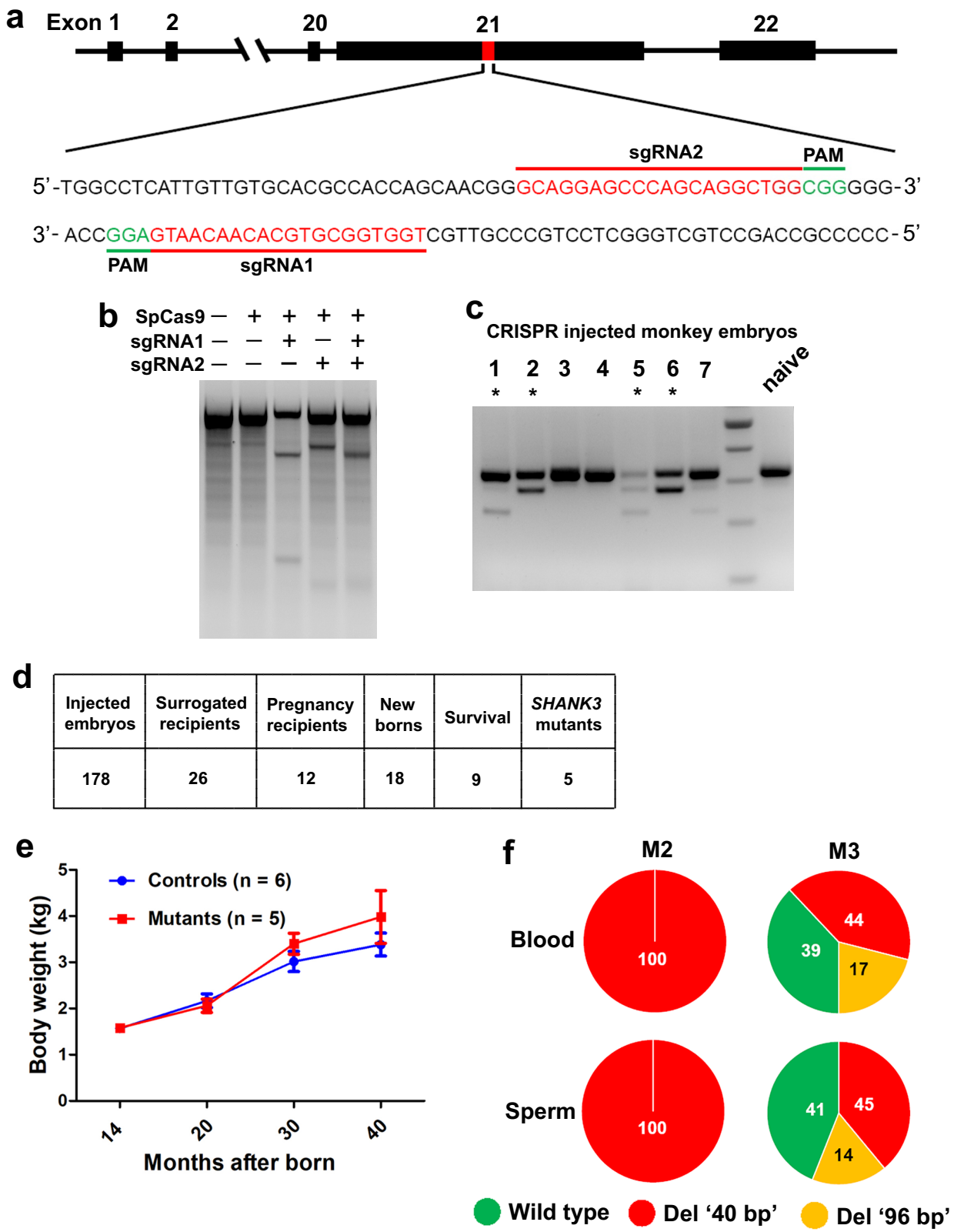

Injected embryos	Surrogated recipients	Pregnancy recipients	New borns	Survival	*SHANK3* mutants
178	26	12	18	9	5

Extended Data Fig. 2 | Summary of founder and germline-transmitted *SHANK3* mutations. a, Schematic showing the structure of the wild-type macaque *SHANK3* gene and magnified panels with the annotated sequence of the gRNA and protospacer adjacent motif (PAM) for both strands within exon 21. **b**, SURVEYOR assay showing *Sp*Cas9-mediated indels in cultured cynomolgus monkey primary skin fibroblasts with indicated gRNAs. **c**, Genotyping PCR results of individual monkey embryos injected with a mixture of Sp*Cas9* mRNA, *SHANK3* gRNA no. 1 and gRNA no. 2. Asterisks indicate effectively edited embryos. **d**, Number of injected embryos, transferred recipients and newborn macaques in this study. **e**, *SHANK3*-mutant macaques have similar body weights to those of age-matched wild-type controls. **f**, Pie charts of genotype (indels) of DNA from semen from mutant macaques M2 and M3 show a similar pattern to their respective blood samples.

Extended Data Fig. 3 | Alignment of partial *SHANK3* sequence genotyped from skin DNA. a–e, Alignment of ten representative reads of *SHANK3* sequence genotyped from a skin biopsy of each mutant monkey with reference *SHANK3* sequence from wild-type monkey.

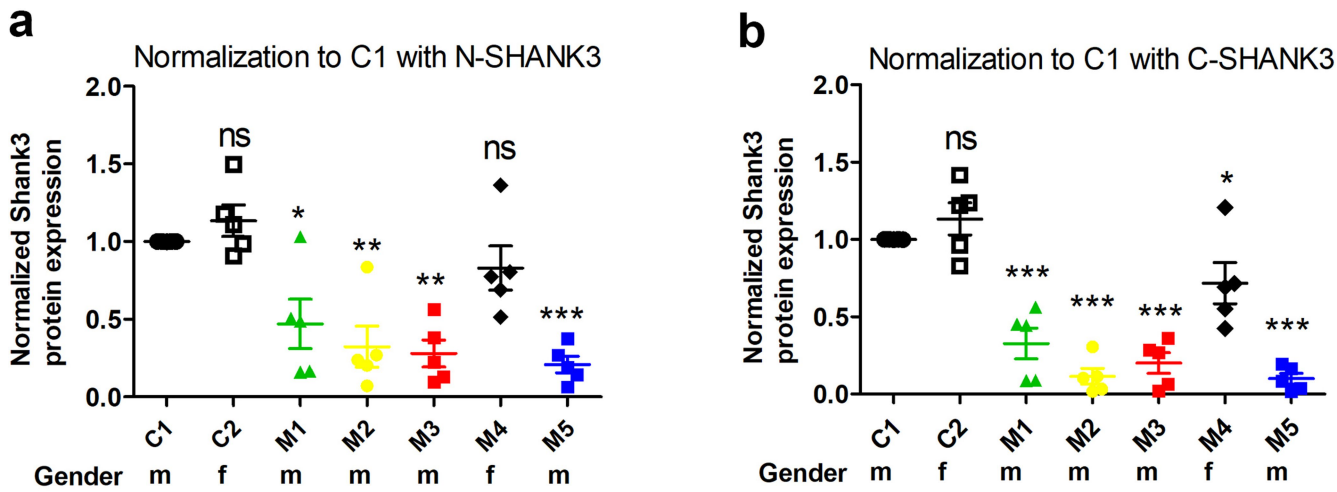

Extended Data Fig. 4 | Statistical analysis of western blots using brain lysates prepared from V1 biopsy of macaques. a, **b**, Quantification of blots was based on five technical repeats using the same V1 protein sample with N-terminal **(a)** and C-terminal **(b)** antibodies. Values were normalized to those of the C1 control monkey. α-Tubulin, as loading control, was run on the same gel. Data are presented as mean ± s.e.m., $n = 5$ technical repeats using sample for the 2 controls and 5 *SHANK3* mutants, $^{*}P < 0.05$, $^{**}P < 0.01$, $^{***}P < 0.001$; ns, not significant; one-way analysis of variance (ANOVA) with Bonferroni post hoc test.

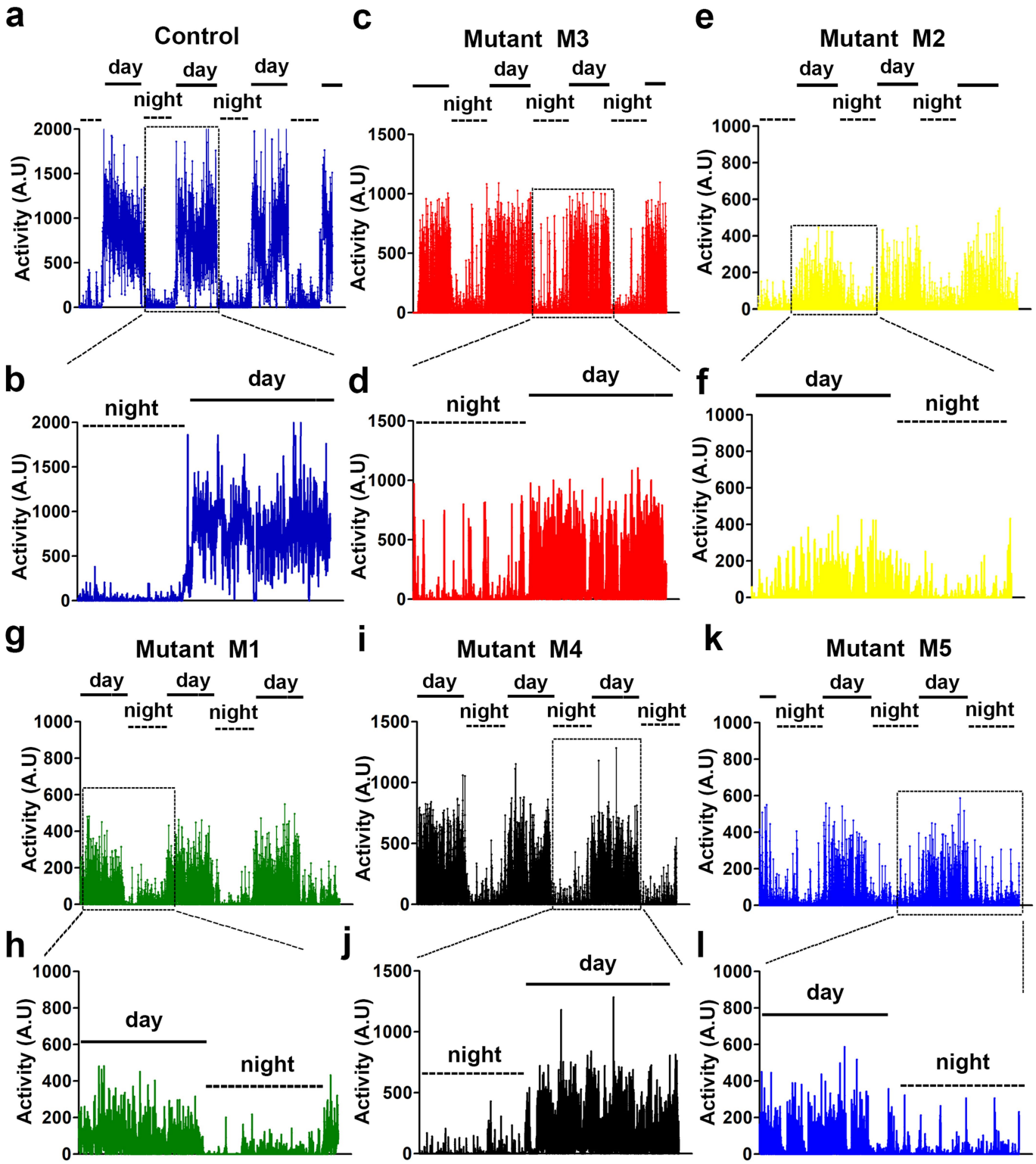

Extended Data Fig. 5 | Representative traces of overall activity. a–l, Representative and enlarged traces of overall activity recorded by motion watches across multiple days from a control macaque and all five SHANK3 mutants. A.U, arbitrary units.

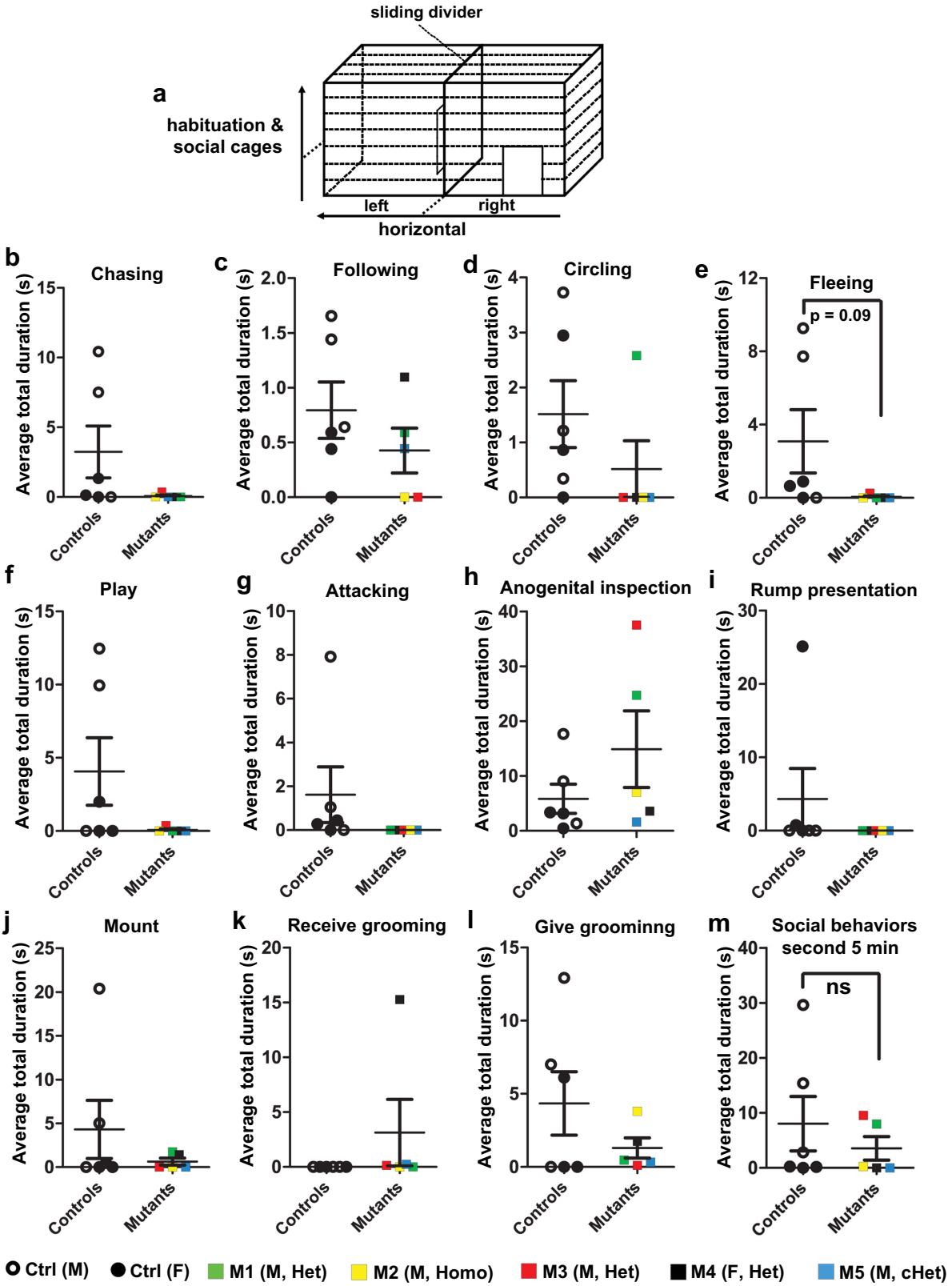

Extended Data Fig. 6 | Behavioural parameters of monkeys during the first and second five minutes of interaction. a, Schematic showing the two interconnected cages used for habituation of individual macaques and subsequent paired social-interaction assay. **b**–**l**, Separate behavioural parameters of monkeys in control and *SHANK3*-mutant groups during the first five minutes of interaction. **m**, No difference in social behaviours (including chasing, following, circling, fleeing and play) during the second five minutes of interaction. In all panels, $n = 6$ macaques for control group; $n = 5$ macaques for the *SHANK3*-mutant group. Data are presented as mean ± s.e.m., two-tailed Mann–Whitney *U*-test.

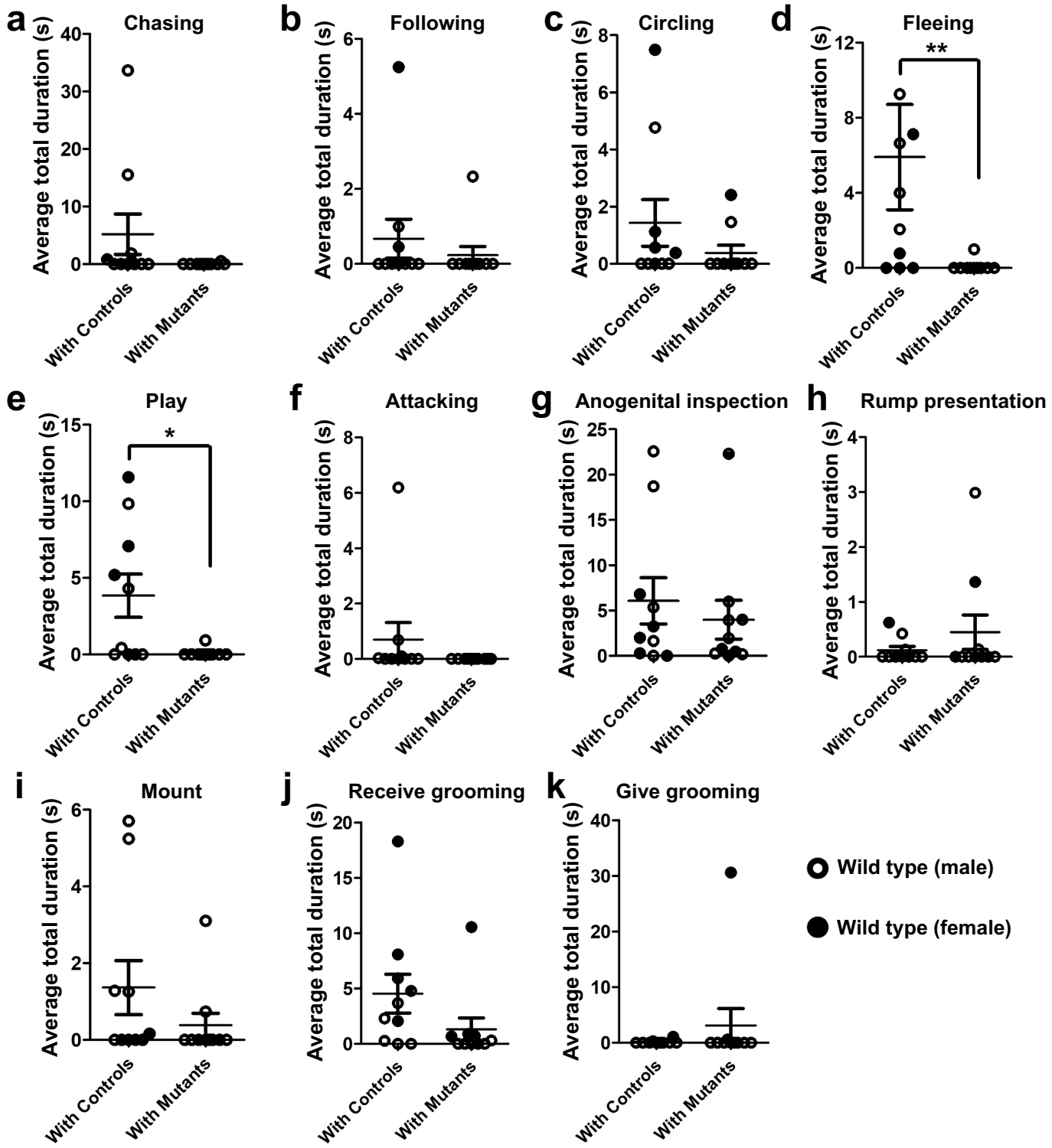

Extended Data Fig. 7 | Behavioural parameters of probe macaques when paired with wild-type or *SHANK3*-mutant monkeys during the first five minutes of interaction. a–k, Total durations of chasing (**a**), following (**b**), circling (**c**), fleeing (**d**), play (**e**), attacking (**f**), anogenital inspection (**g**), rump presentation (**h**), mounting (**i**), receiving grooming (**j**) and giving grooming (**k**). In all panels, $n = 10$ probe monkeys paired individually with 6 wild-type macaques from the control group and 5 macaques from the *SHANK3*-mutant group. Data are presented as mean ± s.e.m., $^{*}P < 0.05$, $^{**}P < 0.01$; two-tailed Mann–Whitney *U*-test.

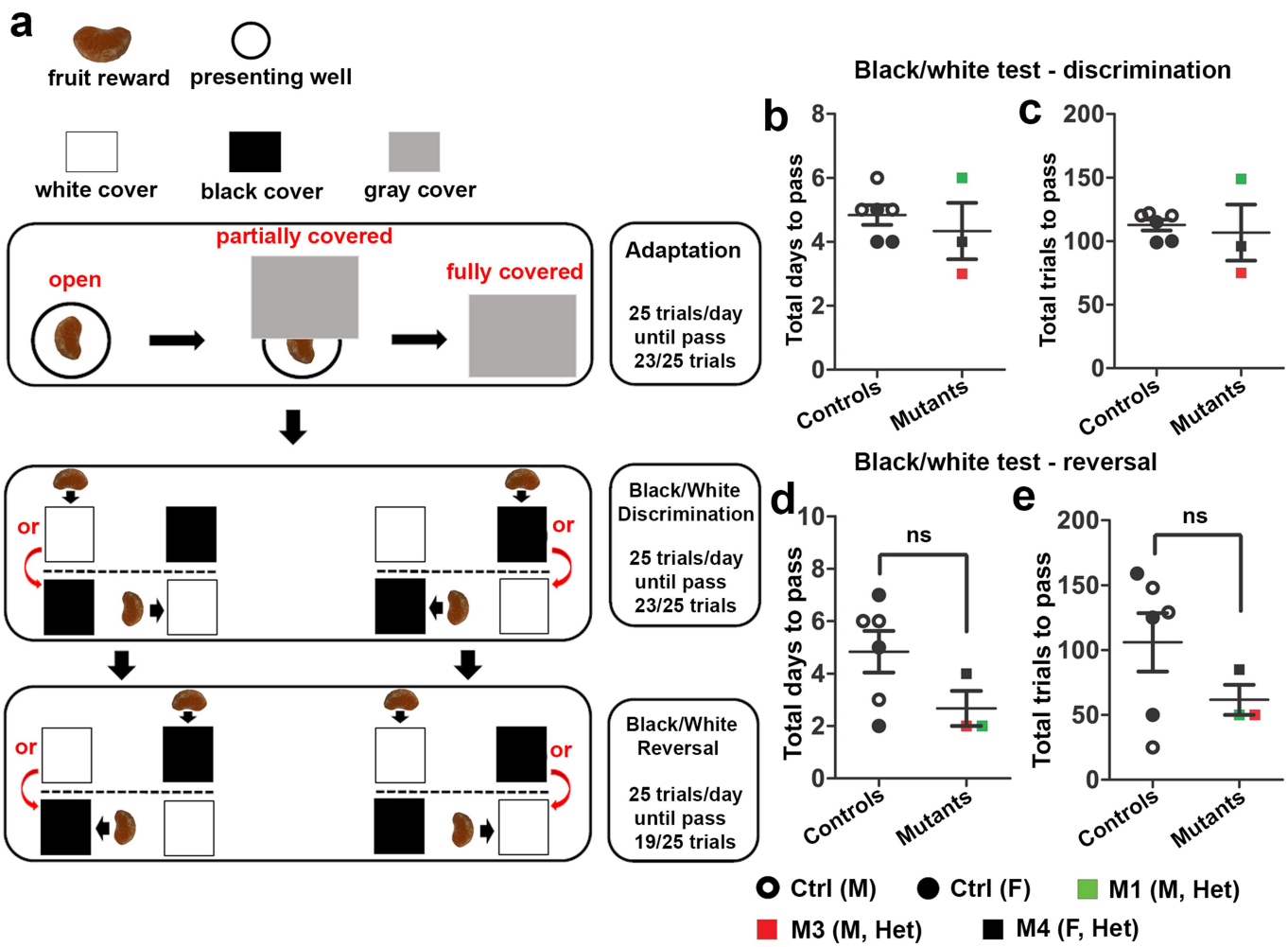

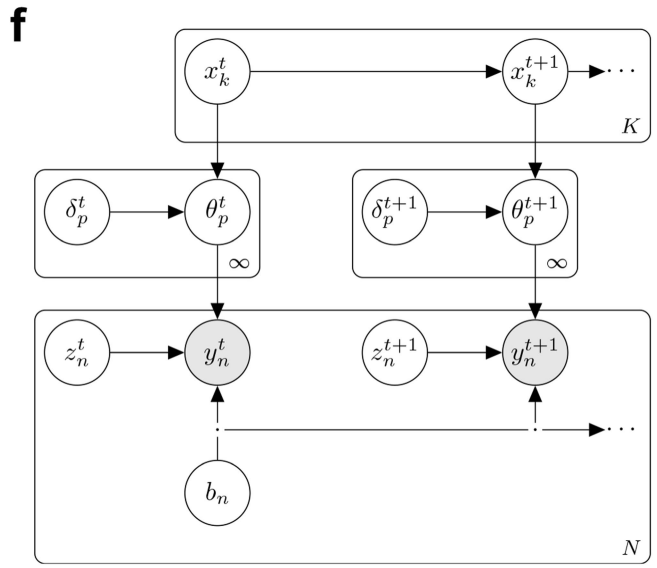

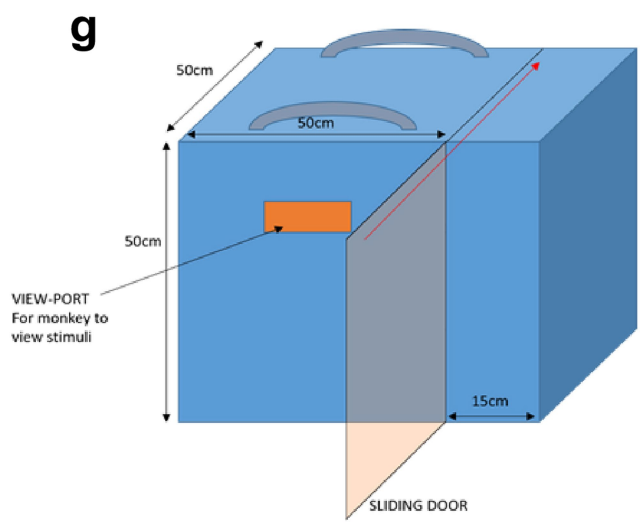

Extended Data Fig. 8 | Performance of control and mutant monkeys in the discrimination and reversal tasks using WGTA. a, Task design. **b**, **c**, Total days (**b**) and total trials (**c**) required for macaques to pass the black–white discrimination test of the WGTA. **d**, **e**, Total days (**d**) and total trials (**e**) required for macaques to pass the black–white reversal test of the WGTA (>75%-correct trial). **f**, A graphical model for Bayesian nonparametric multitarget tracking. Priors omitted for brevity. Arrows pointing to ellipses indicate continuation to the next time step. **g**, Diagram of the eye-tracking box. In **b**–**e**, $n = 6$ macaques for control group; $n = 3$ macaques for the *SHANK3*-mutant group. Data are presented as mean ± s.e.m.; Mann–Whitney *U*-test. Coloured squares indicate individual macaques with *SHANK3* mutations.

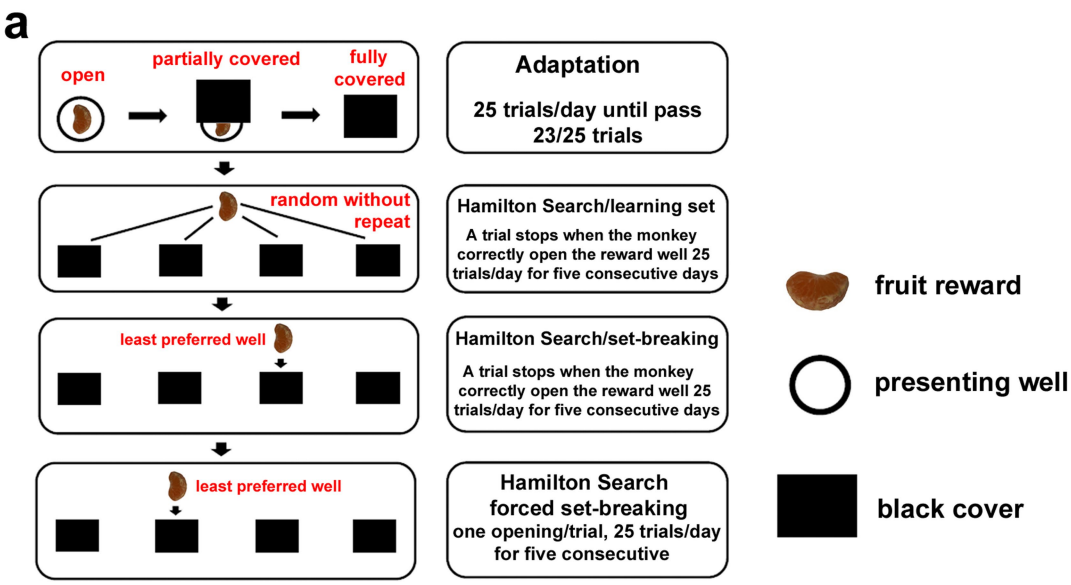

b Hamilton search/set-breaking

monkey ID	C1	C2	C3	C4	C5	C6	M1	M3	M4
maximum	8	21	8	14	13	17	22	5	15
delta	6	20	8	3	12	13	13	0	5

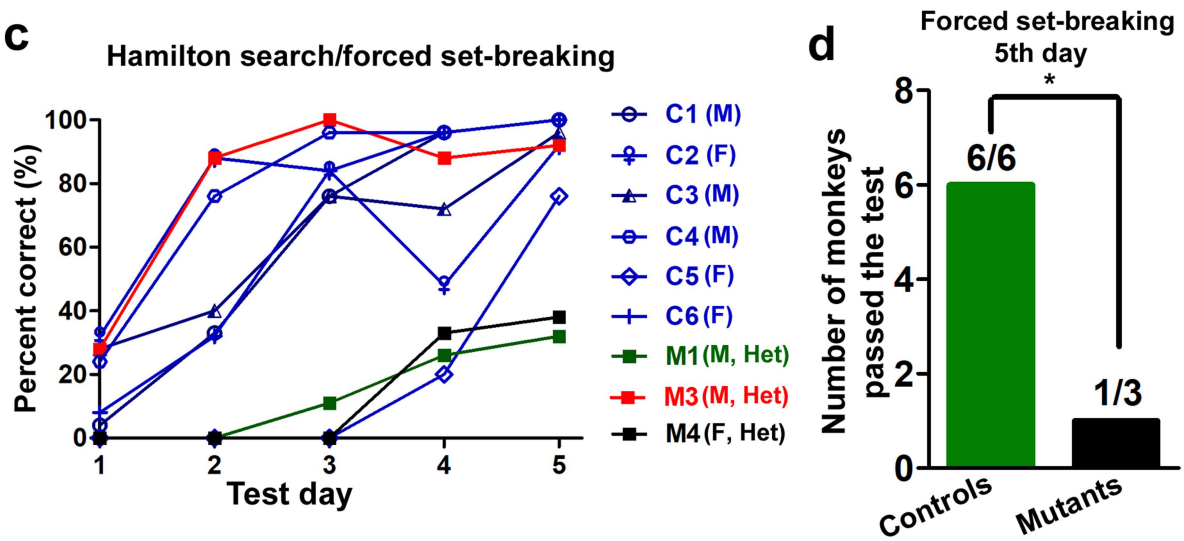

Extended Data Fig. 9 | Performance of controls and SHANK3 mutants in the Hamilton search task. a, Schematic and flow chart of the Hamilton search task. **b**, Performance of macaques in the 'set-breaking' test of the Hamilton search task. M3 showed no improvement (delta value = 0). 'Delta' is set to measure the learning of the monkey across five test days, calculated by increase of the number of trials in which the monkey opened the correct well on the first try. **c**, Percentage of correct trials on the 'forced set-breaking' test of the Hamilton search task, from monkeys across five test days. **d**, Number of monkeys that reached a 75%-correct rate on the fifth day of the forced set-breaking test. $^{*}P < 0.05$, Two-tailed χ^2 test ($P = 0.023$) was applied to determine the statistical difference between groups.

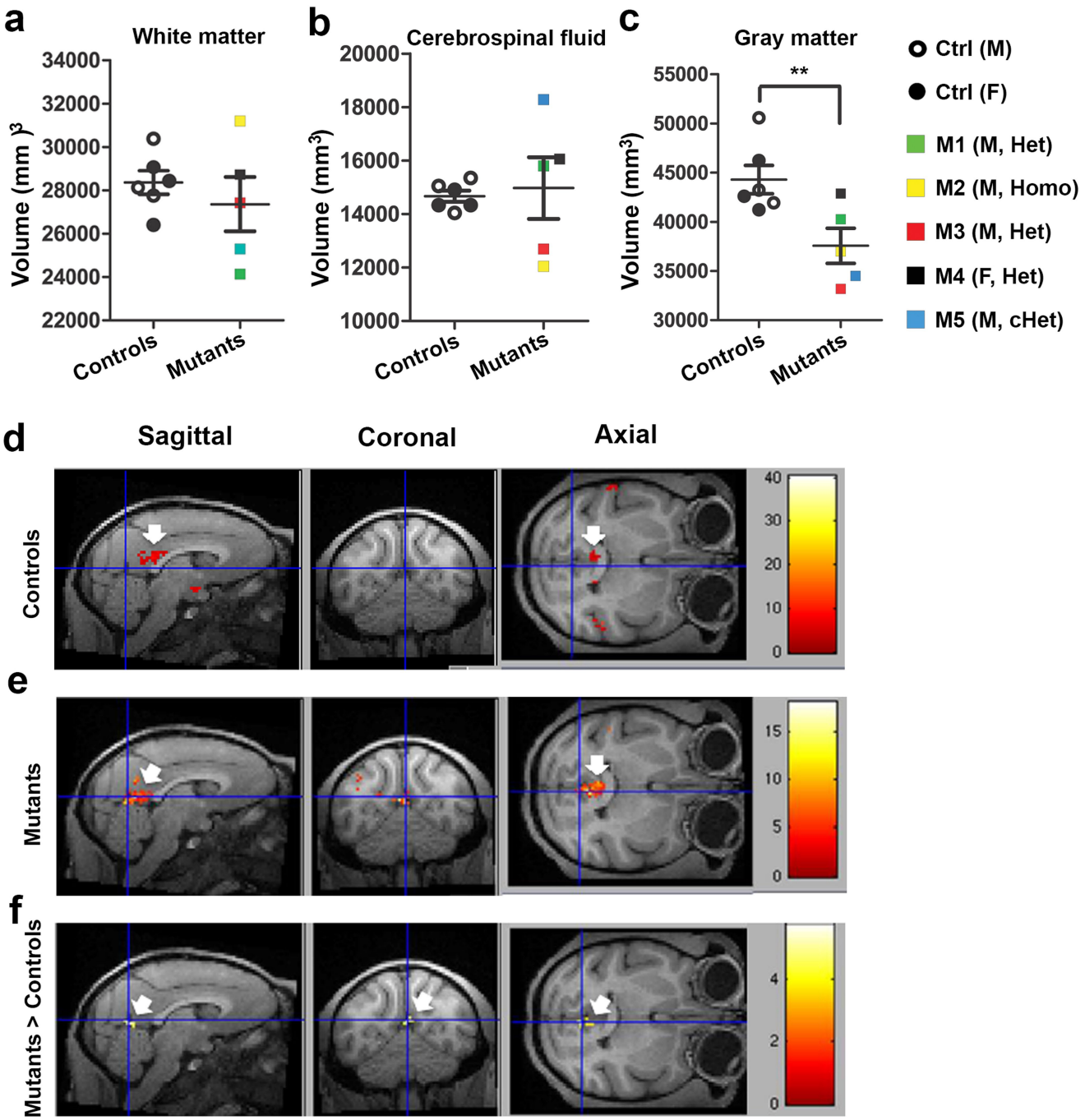

Extended Data Fig. 10 | Structural MRI and seed-based functional MRI analysis of macaque brains. a–c, No difference in white matter volume (**a**) and cerebrospinal fluid volume (**b**), but a reduced volume of grey matter (**c**), in *SHANK3* mutants, relative to control macaques. In **a–c**, $n = 6$ macaques for control group; $n = 5$ macaques for *SHANK3*-mutant group. Data are presented as mean ± s.e.m., $^{**}P < 0.01$, Mann–Whitney *U*-test. Coloured squares indicate individual mutant macaques. **d**, **e**, Sagittal, coronal and axial views of averaged functional MRI image from six control macaques (**d**) and five *SHANK3* mutants (**e**), using the putative posterior cingulate cortex as seed region. **f**, Sagittal, coronal and axial views of averaged functional MRI image show blood-oxygen-level-dependent signals in the posterior cingulate cortex that are greater in mutants than in controls. In **d** –**f**, the putative posterior cingulate cortex regions are highlighted by arrows.

nature research

Corresponding author(s): Feng, G; Yang, S; Xiang, AP; Zhou, H

Reporting Summary

Nature Research wishes to improve the reproducibility of the work that we publish. This form provides structure for consistency and transparency in reporting. For further information on Nature Research policies, see Authors & Referees and the Editorial Policy Checklist.

Statistical parameters

When statistical analyses are reported, confirm that the following items are present in the relevant location (e.g. figure legend, table legend, main text, or Methods section).

n/a	Confirmed	
☐	☒	The exact sample size (*n*) for each experimental group/condition, given as a discrete number and unit of measurement
☐	☒	An indication of whether measurements were taken from distinct samples or whether the same sample was measured repeatedly
☐	☒	The statistical test(s) used AND whether they are one- or two-sided *Only common tests should be described solely by name; describe more complex techniques in the Methods section.*
☒	☐	A description of all covariates tested
☒	☐	A description of any assumptions or corrections, such as tests of normality and adjustment for multiple comparisons
☒	☐	A full description of the statistics including central tendency (e.g. means) or other basic estimates (e.g. regression coefficient) AND variation (e.g. standard deviation) or associated estimates of uncertainty (e.g. confidence intervals)
☒	☐	For null hypothesis testing, the test statistic (e.g. *F*, *t*, *r*) with confidence intervals, effect sizes, degrees of freedom and *P* value noted *Give P values as exact values whenever suitable.*
☒	☐	For Bayesian analysis, information on the choice of priors and Markov chain Monte Carlo settings
☐	☒	For hierarchical and complex designs, identification of the appropriate level for tests and full reporting of outcomes
☒	☐	Estimates of effect sizes (e.g. Cohen's *d*, Pearson's *r*), indicating how they were calculated
☐	☒	Clearly defined error bars *State explicitly what error bars represent (e.g. SD, SE, CI)*

Our web collection on statistics for biologists may be useful.

Software and code

Policy information about availability of computer code

Data collection	Standard programs were used
Data analysis	Prism 5 was used for statistical analysis in this study

For manuscripts utilizing custom algorithms or software that are central to the research but not yet described in published literature, software must be made available to editors/reviewers upon request. We strongly encourage code deposition in a community repository (e.g. GitHub). See the Nature Research guidelines for submitting code & software for further information.

Data

Policy information about availability of data

All manuscripts must include a data availability statement. This statement should provide the following information, where applicable:

- Accession codes, unique identifiers, or web links for publicly available datasets
- A list of figures that have associated raw data
- A description of any restrictions on data availability

All data are available in the main text or the supplementary materials. All sequencing data, images, code, and materials used in the analysis are available to researchers for the purpose of reproducing or extending the analyses

Field-specific reporting

Please select the best fit for your research. If you are not sure, read the appropriate sections before making your selection.

☒ Life sciences ☐ Behavioural & social sciences ☐ Ecological, evolutionary & environmental sciences

For a reference copy of the document with all sections, see nature.com/authors/policies/ReportingSummary-flat.pdf

Life sciences study design

All studies must disclose on these points even when the disclosure is negative.

Sample size	No statistical calculations were applied to pre-determine sample size, but our sample sizes are similar to those reported in previous publications (reference # 18: Liu et al., Nature 2016 and reference # 19: Chen et al., Cell 2017).
Data exclusions	No data point from any behavioral or image assays was excluded for all results reported in this study.
Replication	All experimental findings were reliably reproduced among all subjects in all experiments.
Randomization	SHANK3 mutant animals were allocated based on availability after genetic engineering; wild-type control animals were allocated based upon age, and gender similarity to mutants. Randomization of animals and groups were applied throughout all behavioral and MRI assays in the study.
Blinding	All behavioral observations, scoring, data analysis in this study were carried out by trained researchers without prior knowledge of the experimental design and goal of this study. MRI image analysis was relied on objective, automatized measurements, and investigators were blinded to group allocation during data collection and analysis.

Reporting for specific materials, systems and methods

Materials & experimental systems

n/a	Involved in the study
☒	☐ Unique biological materials
☐	☒ Antibodies
☒	☐ Eukaryotic cell lines
☒	☐ Palaeontology
☐	☒ Animals and other organisms
☒	☐ Human research participants

Methods

n/a	Involved in the study
☒	☐ ChIP-seq
☒	☐ Flow cytometry
☐	☒ MRI-based neuroimaging

Antibodies

Antibodies used	We utilized N-SHANK3 antibody (1:100 from NIH NeuroMab N367/62), C-SHANK3 antibody (1: 500 from Santa Cruz Biotech SC-30193), and Beta-Tubulin antibody (1: 5000 from Sigma T8328) as primary antibodies. We used goat-anti-mouse IRDye 680 (1: 5000 from Li-COR Biosciences), donkey-anti-rabbit IRDye 800CW (1: 5000 from Li-COR Biosciences) as secondary antibodies.
Validation	All antibodies utilized in this study were previously validated in the reference # 26: Zhou et al. Neuron 2016. Li-COR Odyssey Image Studio software was used to image blots and to quantify the intensity of band automatically. Detailed information of each antibody is listed below: N-SHANK3 antibody (1:100 from NIH NeuroMab N367/62) http://neuromab.ucdavis.edu/datasheet/N367_62.pdf C-SHANK3 antibody (1: 500 from Santa Cruz Biotech SC-30193)http://datasheets.scbt.com/sc-30193.pdfBeta-Tubulin antibody (1: 5000 from Sigma T8328) https://www.sigmaaldrich.com/catalog/product/sigma/t8328?lang=en&region=USGoat-anti-mouse IRDye 680 (1: 5000 from Li-COR Biosciences)https://www.licor.com/documents/802khe2qs9bdcb7k88p9Donkey-anti-rabbit IRDye 800CW (1: 5000 from Li-COR Biosciences) https://www.licor.com/bio/products/reagents/secondary_antibodies/irdye_800cw.html

Animals and other organisms

Policy information about studies involving animals; ARRIVE guidelines recommended for reporting animal research

Laboratory animals	Juvenile and adult Cynomolgus monkeys (Macaca fascicularis) in both genders were utilized in this study.

Wild animals	The study did not involve wild animals.
Field-collected samples	The study did not involve samples collected from fields.

Magnetic resonance imaging

Experimental design

Design type	Resting state functional and structural MRI under anesthesia
Design specifications	In all subjects, the slices for functional MRI were acquired using contiguous, interleaved acquisition; 128 volumes per run (3 consecutive runs, each lasting approximately 5 minutes).
Behavioral performance measures	No behavioral measure were taken

Acquisition

Imaging type(s)	Structural and functional
Field strength	3 Tesla
Sequence & imaging parameters	MP-RAGE and T2*weighted gradient echo, echo planar imaging. Following parameters were used - volume repetition time (TR) = 2.1 s, echo time (TE) = 25ms, flip angle = 90°, 1.25mm x 1.25mm in plane resolution and slice thickness = 1.3mm). T1-weighted, magnetization-prepared rapid gradient echo (MP-RAGE) structural images were also acquired (TR = 2.1s; TE = 3.21ms, flip angle = 8°, 0.5mm isotropic voxels)
Area of acquisition	Whole brain

Diffusion MRI ☐ Used ☒ Not used

Preprocessing

Preprocessing software	SPM8, CONN toolbox
Normalization	Data were spatially normalized using segmentation routine in SPM8 to structural scans. Mutual information Affine registration was used for alignment; B-Spline interpolation was used for writing normalized images.
Normalization template	We used MNI Cynmologous macaque atlas as structural templates (purl.org/net/kbmd/cyno).
Noise and artifact removal	Artifact rejection toolbox (ART; www.nitrc.org/projects/artifact_detect) was used for a comprehensive analysis of sources of artifacts in time series data including spiking and motion. Maximum motion (Controls=0.09±0.01 vs. mutants=0.099±0.01; p=0.66); mean motion (controls 0.036 +/- 0.01; mutants 0.036 +/- 0.01; p=0.48). The physiological noise correction was implemented through an anatomical component based noise correction approach (aCompCor) which involves removal of first 3 principal components of the signal from white matter and CSF
Volume censoring	For volume censoring outlier data points (TRs) were defined as volumes that exceeded three z-normalized standard deviations away from mean global brain activation across the entire volume or a composite movement threshold of 0.5 mm scan-to-scan frame-wise displacement.

Statistical modeling & inference

Model type and settings	For resting state local and global functional connectivity analysis, we employed an unbiased data driven approach. Integrated Local Correlation (ILC) was used to assess coupling of local neuronal processes in any given voxel's neighborhood. ILC maps represent a measure of local coherence at each voxel, characterized by the average correlation between each individual voxel and a region of neighboring voxels. For both ILC and GCOR, first-level correlation maps were produced by extracting denoised time series by regressing non-BOLD components from each voxel to the rest of the voxels, followed by computing Pearson's correlation coefficients (r) between that time course and the time course of all other voxels. Correlation coefficients were converted to normally distributed z-scores using Fisher's r-to-z transformation to perform second-level General Linear Model (GLM) analyses. These second-level within group and between-group t-tests were performed for the correlation maps for both controls and mutants (https://sites.google.com/view/conn/measures/networks-voxel-level).
Effect(s) tested	There were no tasks or stimulus conditions. Global Correlation (GCOR) and Local correlations (ILC) were used for resting state functional connectivity analysis. GCOR maps provide a voxel by voxel measure of network centrality, characterized by the strength and sign of functional connectivity between a given voxel and every other voxel in the brain. ILC maps represent a measure of local coherence at each voxel, characterized by the average correlation between each individual voxel and a region of neighboring voxels.

Specify type of analysis: ☒ Whole brain ☐ ROI-based ☐ Both

Statistic type for inference (See Eklund et al. 2016)	Voxel to voxel analysis.
Correction	Height threshold = p< 0.005 and cluster threshold = p< 0.05 (corrected for false discovery rate)

Models & analysis

n/a	Involved in the study
☐	☒ Functional and/or effective connectivity
☒	☐ Graph analysis
☒	☐ Multivariate modeling or predictive analysis

Functional and/or effective connectivity

For resting state local and global functional connectivity analysis, we employed an unbiased data driven approach. Integrated Local Correlation (ILC) was used to assess coupling of local neuronal processes in any given voxel's neighborhood. ILC maps represent a measure of local coherence at each voxel, characterized by the average correlation between each individual voxel and a region of neighboring voxels.

For both ILC and GCOR, first-level correlation maps were produced by extracting denoised time series by regressing non-BOLD components from each voxel to the rest of the voxels, followed by computing Pearson's correlation coefficients (r) between that time course and the time course of all other voxels. Correlation coefficients were converted to normally distributed z-scores using Fisher's r-to-z transformation to perform second-level General Linear Model (GLM) analyses. These second-level within group and between-group t-tests were performed for the correlation maps for both controls and mutants (https://sites.google.com/view/conn/measures/networks-voxel-level).